Development/Plasticity/Repair

Revisiting the Potency of Tbx2 Expression in Transforming Outer Hair Cells into Inner Hair Cells at Multiple Ages In Vivo

Zhenghong Bi,[1] Minhui Ren,[1,2] Yu Zhang,[3,4] Shunji He,[1] Lei Song,[3,4] Xiang Li,[1] and Zhiyong Liu[1,2,5]

[1]Institute of Neuroscience, State Key Laboratory of Neuroscience, CAS Center for Excellence in Brain Science and Intelligence Technology, Chinese Academy of Sciences, Shanghai 200031, China, [2]University of Chinese Academy of Sciences, Beijing 100049, China, [3]Department of Otolaryngology-Head and Neck Surgery, Ninth People's Hospital, Shanghai Jiao Tong University School of Medicine, Shanghai 200125, China, [4]Ear Institute, Shanghai Jiao Tong University School of Medicine, Shanghai 200125, China, and [5]Shanghai Center for Brain Science and Brain-Inspired Intelligence Technology, Shanghai 201210, China

The mouse auditory organ cochlea contains two types of sound receptors: inner hair cells (IHCs) and outer hair cells (OHCs). Tbx2 is expressed in IHCs but repressed in OHCs, and neonatal OHCs that misexpress Tbx2 transdifferentiate into IHC-like cells. However, the extent of this switch from OHCs to IHC-like cells and the underlying molecular mechanism remain poorly understood. Furthermore, whether Tbx2 can transform fully mature adult OHCs into IHC-like cells is unknown. Here, our single-cell transcriptomic analysis revealed that in neonatal OHCs misexpressing Tbx2, 85.6% of IHC genes, including *Slc17a8*, are upregulated, but only 38.6% of OHC genes, including *Ikzf2* and *Slc26a5*, are downregulated. This suggests that Tbx2 cannot fully reprogram neonatal OHCs into IHCs. Moreover, Tbx2 also failed to completely reprogram cochlear progenitors into IHCs. Lastly, restoring Ikzf2 expression alleviated the abnormalities detected in Tbx2+ OHCs, which supports the notion that Ikzf2 repression by Tbx2 contributes to the transdifferentiation of OHCs into IHC-like cells. Our study evaluates the effects of ectopic Tbx2 expression on OHC lineage development at distinct stages of either male or female mice and provides molecular insights into how Tbx2 disrupts the gene expression profile of OHCs. This research also lays the groundwork for future studies on OHC regeneration.

Key words: **cochlea; Ikzf2; inner hair cells; inner ear; outer hair cells; Tbx2**

Significance Statement

Elucidation of the molecular and genetic mechanisms governing the determination and stability of cochlear inner hair cells (IHCs) and outer hair cells (OHCs) should provide valuable insights into the regeneration of damaged IHCs and OHCs. Here, we conditionally overexpress Tbx2 in vivo in cochlear sensory progenitors, neonatal OHCs, or adult OHCs. Our results show that Tbx2 overexpression alone can partially destabilize the OHC fate but cannot fully convert OHCs into IHCs. Specifically, we demonstrate that Ikzf2 repression due to Tbx2 overexpression is one of the key pathways disrupting the OHC fate.

Introduction

Understanding how lineage-specific or -determining transcription factors (TFs), such as MyoD for muscle and Ascl1 for nerve, function is a critical research goal in the developmental biology field (Gurdon et al., 2020). This effort is expected to provide new molecular and genetic insights into how each cell type is specified and maintained and could potentially identify methods to regenerate cell populations absent after damage. The mammalian auditory organ, the cochlea, contains two types of sound receptors known as hair cells (HCs), the inner HCs (IHCs) and outer HCs (OHCs; Morsli et al., 1998). Whereas OHCs but not IHCs express Prestin (encoded by *Slc26a5*; Zheng et al., 2000;

Received Sept. 17, 2023; revised Jan. 30, 2024; accepted March 24, 2024.

Author contributions: Z.L. designed research; Z.B., Y.Z., S.H., and X.L. performed research; Z.B., M.R., Y.Z., L.S., X.L., and Z.L. analyzed data; X.L. and Z.L. wrote the paper.

We thank Dr. Qian Hu of the Optical Imaging Facility of the Institute of Neuroscience (ION) for support with image analysis; Drs. Xu Wang and Yu Kong from the Electronic Microscope Facility of the ION for SEM assistance; and Ms. Qian Liu from the Department of Embryology of the ION animal center for helping us in transplanting zygotes into pseudopregnant female mice. We thank Dr. Jian Zuo (Creighton University, USA) for kindly providing the *Slc26a5*$^{CreER/+}$ strain and Dr. Lin Gan (Augusta University, USA) for the *Atoh1*$^{Cre/+}$ strain. This study was funded by the National Natural Science Foundation of China (32371054, 32321163648, 82101217, 82000985, and 32300811), National Key R&D Program of China (2022ZD0207000, 2020YFE0205900, and 2021YFA1101804), Strategic Priority Research Program of Chinese Academy of Science (XDB32060100), Shanghai Municipal Science and Technology Major Project (2018SHZDZX05), and Innovative Research Team of High-Level Local Universities in Shanghai (SSMU-ZLCX20180601).

The authors declare no competing financial interests.

Correspondence should be addressed to Xiang Li at lixiang@ion.ac.cn or Zhiyong Liu at zhiyongliu@ion.ac.cn.

https://doi.org/10.1523/JNEUROSCI.1751-23.2024

Liberman et al., 2002; Y. Sun et al., 2022), IHCs but not OHCs express vGlut3 (Ruel et al., 2008; Seal et al., 2008). Moreover, multiple subtypes of supporting cells (SCs) are intermingled with IHCs or OHCs (Luo et al., 2021). Both IHCs and OHCs are descendants of Atoh1+ cochlear prosensory progenitors (Matei et al., 2005; Driver et al., 2013). Atoh1 is a master TF essential for cochlear HC production (Tao et al., 2021; Luo et al., 2022), and HC (both IHC and OHC) development is severely defective in *Atoh1*$^{-/-}$ mice (Bermingham et al., 1999; Woods et al., 2004; Fritzsch et al., 2005; Cai et al., 2015; Wang et al., 2021). Notably, although SCs are also derived from progenitors expressing *Atoh1* mRNA (Matei et al., 2005; Driver et al., 2013; S. Li et al., 2022), Atoh1 protein is not detected in SCs. In contrast, Atoh1 protein is strongly and transiently expressed in IHCs and OHCs (S. Li et al., 2022).

Recent genetic studies have revealed how cochlear sensory progenitors differentiate into vGlut3+ IHCs or Prestin+ OHCs. Insm1 and Ikzf2 are both expressed in OHCs, but not in IHCs, and play key roles in early and late OHC development, respectively (Sun and Liu, 2023). Half of the *Insm1*$^{-/-}$ OHCs transdifferentiate into IHC-like cells (Wiwatpanit et al., 2018; S. Li et al., 2023), and *Ikzf2*$^{cello/cello}$ OHCs are dysfunctional and maintain some IHC gene expression (Chessum et al., 2018). Ectopic Ikzf2 can also induce Prestin expression in IHCs and promote the regeneration of Prestin+ OHC-like cells from adult SCs (Chessum et al., 2018; S. Sun et al., 2021). Furthermore, Tbx2 is expressed as early as when the otocyst is formed (Kaiser et al., 2021; Song and Morrow, 2023), and three independent studies have recently shown that Tbx2 is essential for IHC fate specification, differentiation, and maintenance (Bi et al., 2022; Garcia-Anoveros et al., 2022; Kaiser et al., 2022). Briefly, *Tbx2*$^{-/-}$ IHCs transdifferentiate into OHC-like cells. Conversely, neonatal OHCs misexpressing ectopic Tbx2 downregulate Prestin and upregulate vGlut3 expression (Garcia-Anoveros et al., 2022; Kaiser et al., 2022). Moreover, dual expression of Atoh1 transiently and Tbx2 persistently transforms medial SCs at neonatal ages into IHC-like cells in both undamaged and damaged cochleae (Bi et al., 2022; X. Li et al., 2023).

In our current study, we aimed to address three uncertainties relevant to Tbx2: (1) the extent to which Tbx2 overexpression transforms OHCs into IHC-like cells; (2) whether Tbx2 is sufficient to perturbate the gene expression profiles of the adult OHCs; and (3) the molecular mechanisms underlying Tbx2 converts OHCs to IHC-like cells. When Tbx2 was overexpressed in neonatal OHCs, the OHC-to-IHC conversion was incomplete; ~85.6% of IHC genes, including the vGlut3 (*Slc17a8*) gene, were upregulated, but only 38.6% of OHC genes, such as Prestin (*Slc26a5*) and *Ikzf2* genes, were downregulated. Unexpectedly, Tbx2 also appeared to be unable to fully reprogram cochlear progenitors into IHCs. However, Tbx2 was able to perturb the gene expression of adult OHCs. Lastly, Ikzf2 overexpression partially alleviated the abnormalities of the Tbx2+ OHCs. Thus, repression of Ikzf2 expression by Tbx2 is likely a key signaling pathway involved in the switching of OHCs into IHC-like cells.

Materials and Methods

Mice. The mouse strain *Slc26a5*$^{CreER/+}$ was kindly provided by Dr. Jian Zuo (Creighton University; Fang et al., 2012), and *Atoh1*$^{Cre/+}$ was kindly provided by Dr. Lin Gan (Augusta University; Yang et al., 2010). The details of the *Fgf8*$^{GFP/+}$ strain are described in our previous report (Pan et al., 2023). Tamoxifen (TMX; catalog #T5648, Sigma-Aldrich) was dissolved in corn oil (catalog #C8267, Sigma-Aldrich) and administered to mice at the dose of 3 or 9 mg/40 g (body weight) at P2/P3 or P60/P61, respectively. Both male and female mice were used in this study. All mice were bred and raised in an SPF-level animal room, and all animal procedures were performed according to the guidelines (NA-032-2022) of the IACUC of the Institute of Neuroscience (ION), Center for Excellence in Brain Science and Intelligence Technology, Chinese Academy of Sciences.

Generation of Rosa26$^{Tbx2/+}$ *and Rosa26*$^{Tbx2\text{-}Ikzf2/+}$ *strains.* The *Tbx2* conditional overexpression mouse strain *Rosa26*-CAG-Loxp-stop-Loxp-Tbx2*3×HA-P2A-tdTomato (*Rosa26*$^{Tbx2/+}$) was established through homologous recombination mediated by CRISPR/Cas9 in one-cell–stage mouse zygotes, into which *Cas9* mRNA, the targeting vector, and *Rosa26* sgRNA were coinjected. The *Rosa26* sgRNA used was *5′-ACTCCAGTCTTTCTAGAAGA-3′*. The injected zygotes were transplanted into pseudopregnant female mice, which subsequently gave birth to founder 0 (F0) mice. The F0 mice were screened using tail-DNA PCR, and mice with potentially correct gene targeting were bred with WT mice to obtain germline-stable F1 mice. Southern blotting was performed to confirm that the targeting vector was not randomly inserted in the F1 mouse genome. The detailed Southern blotting protocol is described in our previous report (C. Li et al., 2018). The same procedure was also used to generate the strain *Rosa26*-CAG-Loxp-stop-Loxp-Tbx2*3 × HA-P2A-Ikzf2*3 × V5-T2A-EGFP/+ (*Rosa26*$^{Tbx2\text{-}Ikzf2/+}$), except that the targeting vector was distinct from that used for *Rosa26*$^{Tbx2/+}$.

Identical mouse genotyping procedures were applied to *Rosa26*$^{Tbx2/+}$ and *Rosa26*$^{Tbx2\text{-}Ikzf2/+}$. We concurrently used three primers to distinguish between the KI and WT alleles: Forward primer 1 (F1): *5′-AGTCGCTCTGAGTTGTTATCAG-3′*; Reverse primer 1 (R1): *5′-TGAGCATGTCTTTAATCTACCTCGATG-3′*; and Reverse primer 2 (R2): *5′-AGTCCCTATTGGCGTTACTATGG-3′*. The PCR protocol was 95°C for 3 min, followed by 30 cycles of 95°C for 30 s, 60°C for 30 s, and 72°C for 40 s and then a final extension at 72°C for 10 min. Whereas the paired primers F1 and R1 produced a 469 bp fragment from the WT allele, the paired primers F1 and R2 yielded a 412 bp fragment from the KI allele.

Sample processing and immunofluorescence staining. We have previously reported the detailed protocol for inner ear tissue processing (Z. Liu et al., 2010). Briefly, inner ear tissues were dissected out, fixed in fresh 4% paraformaldehyde (PFA) overnight at 4°C, washed thrice the next morning in 1× PBS (10 min each), and decalcified in 120 mM EDTA at room temperature.

The primary antibodies used in this study included anti-HA (rat, 1:200; 11867423001, Roche), anti-Prestin (goat, 1:1,000; sc-22692, Santa Cruz Biotechnology), anti-vGlut3 (rabbit, 1:500; 1,35,203, Synaptic Systems), anti-GFP (chicken, 1:500; ab13970, Abcam), anti-Bcl11b (rat, 1:500; ab18465, Abcam), anti-Otoferlin (mouse, 1:500; ab53233, Abcam), anti-Slc7a14 (rabbit, 1:500; HPA045929, Sigma-Aldrich), anti-Ctbp2 (mouse, 1:200; 6,12,044, BD Biosciences), anti-V5 (mouse, 1:500; MCA1360, Bio-Rad), and anti-Prox1 (rabbit, 1:500; AB5475, Sigma-Aldrich). Nuclei were counterstained with Hoechst 33342 solution (1:1,000; 62249, Thermo Fisher Scientific), and samples were mounted using Prolong Gold antifade medium (P36930; Thermo Fisher Scientific). Images were captured using NiE-A1 Plus, TiE-A1 Plus, and Nikon C2 (Nikon) confocal microscopes. All the confocal settings between control and experimental samples were identical, unless otherwise stated.

Cell number, ribbon synapse, and nuclear diameter quantification and measurement. Each cochlea was divided into three portions, basal, middle, and apical turns of equal length, after total cochlear length was measured by scanning under the 10× lens of a confocal microscope. The surviving cells (OHCs and/or cIHCs) in the control group (Slc26a5-Ai9) and experimental group (Slc26a5-Tbx2) in basal, middle, and apical turns were counted separately at P42 and P120, respectively. The numbers of the Ctbp2+ puncta were used to calculate the ribbon synapse per cell via *z*-stack projections of confocal slices (60×) scanned with 0.41 µm interval that covered the entire cell. Each cell/nuclei from ~300 cells of each type (from three mice) was treated as an independent unit. The mosaic distribution of endogenous OHCs and cIHCs in

Slc26a5-Tbx2 mice enabled us to compare the numbers of Ctbp2+ puncta in cIHCs and OHCs and also the IHCs in the same region, thus minimizing the contribution of cochlear regional differences to the variation in the number of Ctbp2+ puncta. Different confocal slices (60×) covering the same cell were also projected, and the "straight line" tool of the ImageJ software was used to measure the diameter of the nuclei per cell.

To quantify the percentages of vGlut3+/Prestin^{Low} or vGlut3+/Prestin^{-} cIHCs in Slc26a5-Tbx2 mice at P14, P42, P76, and P120, we selected the apical turn because no or very few cIHCs/OHCs were lost here. The percentage was calculated by normalizing the number of vGlut3+/Prestin^{Low} or vGlut3+/Prestin^{-} cIHCs against the total number of tdTomato+ cells in the OHC region, which was the sum of the vGlut3+/Prestin^{Low} or vGlut3+/Prestin^{-} cIHCs. The same method was used to quantify the percentages of vGlut3^{Low}/Prestin^{High} or vGlut3^{High}/Prestin^{Low} cIHCs in Slc26a5-Tbx2 mice in which Tbx2 overexpression was induced at P60/P61.

Bioinformatic analysis. FASTQ files of smart-seq data were aligned to the house mouse reference genome (GRCm38) by using Hisat2 (v2.2.1; Kim et al., 2015). To estimate the expression level of each gene, the raw count was calculated using featureCounts (v2.0.1; Liao et al., 2014), and the normalized value TPM (transcripts per million) was calculated using StringTie (v2.2.1; Pertea et al., 2015). Differentially expressed genes (DEGs) between P42_cIHCs and P30_WT OHCs were identified using DESeq2 (v1.34.0; Love et al., 2014), with these criteria: an absolute value of FC > 4, $p < 0.05$. Genes in the lists in Extended Data Figures 6-1 and 8-1 are ranked according to the averaged TPM value.

R package Seurat (v4.0.6) was used for other downstream analyses (Stuart et al., 2019). Principal component analysis (PCA) was performed using "RunPCA"; clustering, using "FindNeighbors" and "FindClusters"; and dimensional reduction, uniform manifold approximation, and projection (UMAP), using "RunUMAP." All single-cell transcriptomic data de novo generated in this study can be accessed using the number GSE233559.

ABR measurement and SEM analysis. P42 WT and Slc26a5-Tbx2 mice were anesthetized, transferred to a soundproof chamber, and stimulated using sound intensities ranging from 90 to 0 dB SPL at 4, 5.6, 8, 11.3, 16, 22.6, 32, and 45 kHz. The responses were recorded using BioSigRZ software (Tucker-Davis Technologies). The details of the procedure are described in our previous report (C. Li et al., 2018).

Cochlear samples used for SEM analysis were processed using protocols reported in our previous study (S. Sun et al., 2021). Briefly, inner ears were fixed using 2.5% glutaraldehyde (G5882, Sigma-Aldrich) and then decalcified in 50 mM EDTA in 1× PBS. The cochlea was next dissected into three turns, with the HCs being exposed and postfixed with 1% osmium tetroxide (18451, Ted Pella). Lastly, the cochlear samples were treated in a turbomolecular pumped coater (model Q150T ES, Quorum) and scanned using a field-emission SEM instrument (model GeminiSEM 300, Zeiss).

Patch-clamp recording of OHCs and cIHCs. Whole-cell patch-clamp recording at room temperature was conducted using an Axon 200B interfaced with Axon Digidata 1440A by using jClamp software (www.scisoftco.com). The recording was from individual first-row OHCs/cIHCs at the 8–11 kHz region. The extracellular/intracellular solutions and the detailed protocol of the patch-clamp recording have been reported in our previous study (Y. Sun et al., 2022).

NLC was measured using a continuous high-resolution two-sine stimulus protocol, which involved superimposing 10 mV peak amplitude sine waves of 390.6 and 781.2 Hz onto a 300 ms voltage ramp from +150 to −150 mV. The capacitance data were fitted to the first derivative of a two-state Boltzmann function:

$$C_m = Q_{max}\frac{ze}{kT}\frac{b}{(1+b)^2} + C_{lin} \text{ where } b = \exp\left(\frac{-ze(V_m - V_{pkcm})}{kT}\right),$$

where Q_{max} is the maximum nonlinear charge moved, V_{pkcm} or V_h is the voltage at peak capacitance, V_m is membrane potential, z represents valence, C_{lin} corresponds to linear membrane capacitance, e is electron charge, k represents Boltzmann's constant, and T is the absolute temperature.

Statistical analysis. Statistical analysis in this study was performed using GraphPad Prism version 8.0.2 (GraphPad Software). All of the data were presented as mean ± SEM. We performed either Student's t tests (two groups) or one-way ANOVA (more than two groups). A statistically significant difference was set at $^{*}p < 0.05$, $^{**}p < 0.01$, $^{***}p < 0.001$, and $^{****}p < 0.0001$ and was indicated in the results and figure legends.

Results

Generation of new conditional *Tbx2* overexpression mouse line

To induce ectopic Tbx2 expression effectively and conditionally in different cell types or at distinct ages, we established a new mouse strain, *Rosa26*-CAG-Loxp-stop-Loxp-Tbx2*3×HA-P2A-tdTomato (*Rosa26*$^{Tbx2/+}$ in brief). In *Rosa26*$^{Tbx2/+}$, the use of the 2A strategy allowed tightly paired expression of Tbx2 and tdTomato (Fig. 1*A–C*). Southern blotting confirmed that the targeting vector was not randomly inserted in the mouse genome (Fig. 1*D*). The wild-type (WT), heterozygous knockin (KI) *Rosa26*$^{Tbx2/+}$ and homozygous (*Rosa26*$^{Tbx2/Tbx2}$) mice were healthy, fertile, and readily identifiable by tail-DNA PCR (Fig. 1*E*). *Rosa26*$^{Tbx2/+}$ and *Rosa26*$^{Tbx2/Tbx2}$ mice did not exhibit any overt developmental defects.

According to the design we used, upon Cre-mediated recombination, cells expressing Tbx2, which was tagged with three HA fragments at its C-terminus, could also be permanently traced using tdTomato, whose expression facilitates subsequent fate mapping and transcriptomic analysis at single-cell resolution. As described below, we used *Slc26a5*$^{CreER/+}$ to specifically target cochlear OHCs at both postnatal day 2 (P2)/P3 and P60/P61, as well as *Atoh1*$^{Cre/+}$ to target undifferentiated cochlear sensory progenitors at embryonic ages.

Ectopic Tbx2 converts neonatal OHCs into IHC-like cells

To ascertain whether functional Tbx2 can be effectively induced in *Rosa26*$^{Tbx2/+}$, we overexpressed Tbx2 in neonatal cochlear OHCs by crossing the strain with *Slc26a5*$^{CreER/+}$ (Fang et al., 2012). Neonatal OHCs misexpressing Tbx2 decrease Prestin and increase vGlut3 expression (Garcia-Anoveros et al., 2022; Kaiser et al., 2022). Given effective Tbx2 induction, a similar phenotype should be observed in *Slc26a5*$^{CreER/+}$; *Rosa26*$^{Tbx2/+}$ mice (Slc26a5-Tbx2 in brief), but not in the control strain, *Slc26a5*$^{CreER/+}$; *Rosa26*-CAG-Loxp-stop-Loxp-tdTomato (Ai9)/+ (Slc26a5-Ai9 in brief). In Slc26a5-Ai9 cochleae, OHCs were equivalent to WT OHCs, except for expressing tdTomato. Both Slc26a5-Ai9 and Slc26a5-Tbx2 mice were administered tamoxifen at P2/P3 and analyzed at P14, P42, P76, or P120 (Fig. 2*A*, $n = 3$ at each age). In control Slc26a5-Ai9 mice, almost all OHCs were tdTomato+ regardless of when they were analyzed. Thus, the data obtained at P42 were chosen to present as examples here. Three rows of Prestin+ OHCs and one row of vGlut3+ IHCs were regularly aligned at P42 (Fig. 2*B–B*"'). Whereas almost all OHCs were tdTomato+, no IHCs expressed tdTomato, in agreement with the OHC-specific Cre activity of *Slc26a5*$^{CreER/+}$ (Fang et al., 2012).

Conversely, vGlut3 was expressed at high levels but Prestin expression was markedly decreased (Fig. 2*C–C*"', orange arrows) or became undetectable (Fig. 2*C–C*"', orange arrowheads) in all tdTomato (Tbx2)+ OHCs in Slc26a5-Tbx2 mice at P14. We defined these vGlut3+/tdTomato+ OHCs expressing low

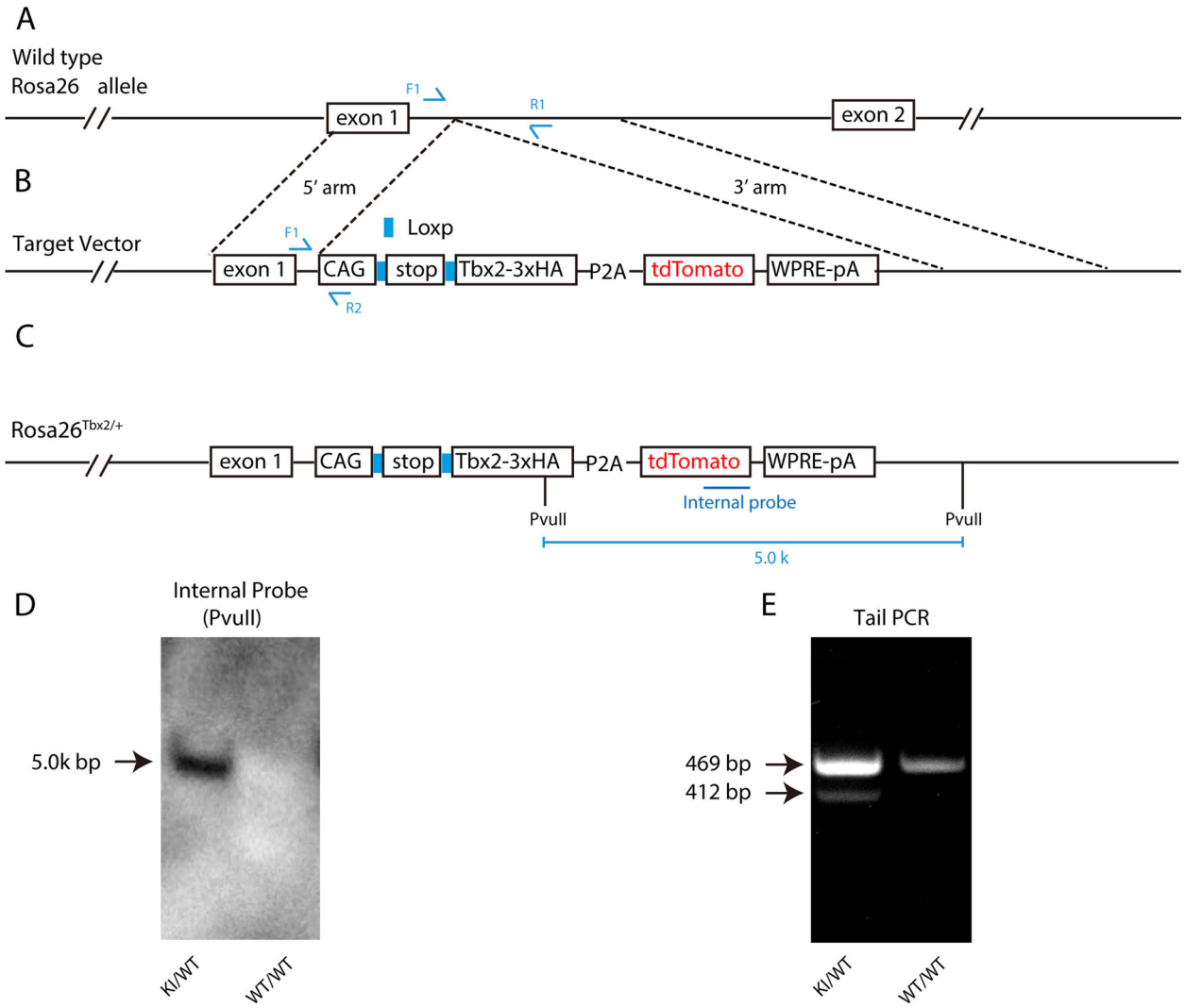

Figure 1. Construction of *Rosa26*-CAG-Loxp-stop-Loxp-Tbx2*3 × HA-P2A-tdTomato (*Rosa26*$^{Tbx2/+}$) strain. ***A–C***, Wild-type *Rosa26* locus. ***A***, Recombined using a targeting vector. ***B***, With 5′ and 3′ homologous arms, generating the post-targeted *Rosa26*$^{Tbx2/+}$ allele. ***C***, Notably, Tbx2 expression and tdTomato expression are tightly paired. ***D***, Southern blotting performed using an internal probe. A 5k bp band is detected in heterozygous (KI/WT) but not in wild-type (WT/WT) mice. ***E***, One example gel image from tail-DNA PCR of heterozygous and wild-type mice.

(Prestin^{Low}) or no detectable Prestin (Prestin^{-}) as "converted IHCs" (cIHCs) derived from endogenous OHCs. The heterogenous levels of Prestin in cIHCs indicated the various stages of incomplete conversion from OHCs to IHCs or IHC-like cells, with Prestin^{-} cIHCs representing the highest degree of conversion. Notably, the endogenous OHCs not expressing tdTomato (Tbx2) maintained Prestin expression at a level as high as in the OHCs in control mice and, as expected, did not express vGlut3 (Fig. 2*C–C*‴, blue arrows). Moreover, all vGlut3+ cIHCs were tdTomato (Tbx2)+, and vice versa, in Slc26a5-Tbx2 mice. Here, despite the identical tamoxifen treatment, fewer tdTomato+ cells were detected in Slc26a5-Tbx2 mice than in Slc26a5-Ai9 mice, which was likely due to the less efficient transcription of the long polycistronic Tbx2/tdTomato sequence in *Rosa26*$^{Tbx2/+}$ than that of tdTomato alone in Ai9/+ mice. Collectively, our data showed that the Slc26a5-Tbx2 mouse line is an efficient model for inducing cIHCs from neonatal OHCs.

Cell fate switch from OHCs to cIHCs is largely complete by P42

Next, to determine when the cell fate switch from OHCs to cIHCs was complete after Tbx2 induction in OHCs, we further analyzed the Slc26a5-Tbx2 mice at P42 (Fig. 2*D–D*‴), P76 (Fig. 2*E–E*‴), and P120 (Fig. 2*F–F*‴). Briefly, similar phenotypes of cell fate conversion from OHCs to IHCs were observed. We quantified the percentages of vGlut3+/Prestin^{Low} cIHCs (Fig. 2, orange arrows) and vGlut3+/Prestin^{-} cIHCs (Fig. 2, orange arrowheads) at P14, P42, P76, and P120. Because limited or no cIHC/OHC loss occurred in the apical turn after P14 (details in the next section), to simplify the analysis, we focused on the apical turn of the Slc26a5-Tbx2 mice. Our criterion is that the presence of vGlut3 and the absence of Prestin expression would suggest a complete conversion of OHCs into cIHCs.

Among all tdTomato+ cIHCs, the percentage of vGlut3+/Prestin^{Low} cIHCs was 78.52% ± 9.27% at P14 ($n = 3$), markedly (****$p < 0.0001$) dropped to 6.12% ± 3.40% at P42 ($n = 3$), and was nearly zero at P76 ($n = 3$) and P120 ($n = 3$; Fig. 2*G*). Conversely, the percentage of vGlut3+/Prestin^{-} cIHCs was 18.04% ± 8.17% at P14, increased drastically (****$p < 0.0001$) to 93.88% ± 3.40% at P42, and reached nearly 100% at P76 and P120 (Fig. 2*H*). We therefore concluded that, upon Tbx2 induction in neonatal OHCs, reactivation of vGlut3 expression was rapid and all cIHCs expressed a high level of vGlut3 by P14,

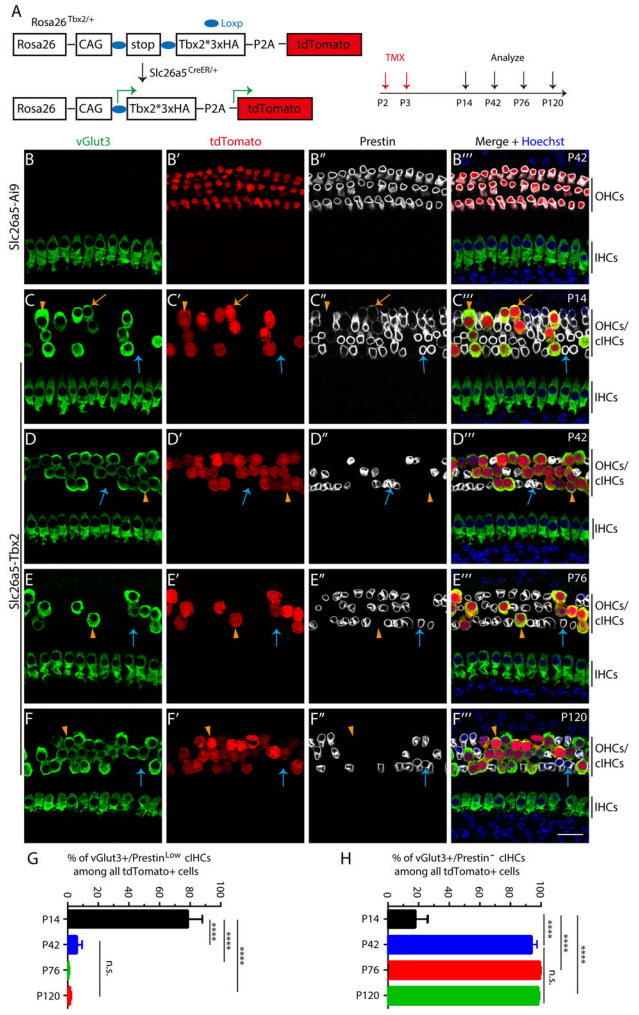

Figure 2. vGlut3 expression is reactivated and Prestin expression is repressed when Tbx2 is ectopically induced in neonatal OHCs. ***A***, Simple illustration of how Tbx2 was specifically overexpressed in neonatal OHCs, which normally do not express Tbx2. ***B–F‴***, Triple labeling for vGlut3, tdTomato, and Prestin in mice with distinct genotypes: Slc26a5-Ai9, at P42 (***B–B‴***); and Slc26a5-Tbx2, at four ages, P14 (***C–C‴***), P42 (***D–D‴***), P76 (***E–E‴***), and P120 (***F–F‴***). Images are captured from the apical turn, where cell death was minimal. Orange arrows: cIHC expressing vGlut3 and low level of Prestin. Orange arrowheads: vGlut3+ cIHCs in which Prestin is undetectable. Blue arrows: endogenous OHCs that maintain high Prestin expression and do not express tdTomato (Tbx2) and vGlut3. ***G***, ***H***, Percentages of cIHCs with high vGlut3 and low Prestin expression (***G***) and cIHCs with high vGlut3 but no detectable Prestin expression (***H***). Data are presented as means ± SEM ($n = 3$ for each age). One-way ANOVA was used for statistical analysis. ****$p < 0.0001$; n.s., not significant. OHCs, outer hair cells; IHCs, inner hair cells; cIHCs, converted inner hair cells. Scale bar: 20 µm (***F‴***).

whereas downregulation of Prestin expression was gradual and a large fraction of cIHCs belonged to the Prestin^{Low} population by P14. Thus, the cell fate conversion process of cIHCs was not synchronized at P14 but mostly completed by P42.

HC loss occurs in Slc26a5-Tbx2 mice after P14

The long-term effects of Tbx2 misexpression on OHCs remain unknown. In control mice at P120 ($n = 3$), HCs were largely intact, with sporadic cell death detected primarily in the basal turn (Fig. 3*A–C*). In contrast, after P14 in Slc26a5-Tbx2 mice, we started to observe the loss of cIHCs or endogenous OHCs in a base-to-apex gradient. The death of endogenous OHCs not expressing Tbx2 was likely a secondary effect due to the degeneration of nearby cIHCs. At P42, the cIHC/OHC loss primarily occurred in the basal turn (Fig. 3*D–F*): 269.33 ± 74.21 ($n = 3$) cells (Prestin+ endogenous OHCs and vGlut3+ cIHCs) existed in the basal turn of Slc26a5-Tbx2 mice, significantly (**$p < 0.01$) fewer than the 649.67 ± 23.70 ($n = 3$) Prestin+ OHCs in the basal turn of Slc26a5-Ai9 mice (Fig. 3*J*).

The cell death we observed not only extended into the middle turn but also became more severe in Slc26a5-Tbx2 cochleae at P120 (Fig. 3*G,H*); however, the cell death in the apical turn remained mild in Slc26a5-Tbx2 mice at P120 (Fig. 3*I*). We separately counted the OHCs/cIHCs in the three turns. There were 580.00 ± 16.50, 157.67 ± 39.33, and zero OHCs/cIHCs present in apical, middle, and basal turns in Slc26a5-Tbx2 mice at P120 ($n = 3$), respectively, which were significantly less than that (705.67 ± 24.40, 770.00 ± 25.24, and 628.33 ± 20.28) in the corresponding turns in Slc26a5-Ai9 mice at P120 ($n = 3$; Fig. 3*K*).

Notably, the IHCs in all three turns were normal at P42. In contrast, severe IHC death occurred in the basal and middle turns, but not the apical turn, at P120, which again was likely due to a secondary effect of cIHC/OHC loss. To support this, a similar IHC death pattern is observed in the *Slc26a5*$^{DTR/+}$ model where OHCs are specifically damaged (S. Sun et al., 2021). Collectively, in the presence of ectopic Tbx2, neonatal OHCs would become cIHCs that, however, began to degenerate after P14.

cIHCs also gain other IHC features and lose Ikzf2 expression

We next determined whether cIHCs expressed other IHC markers or gained additional IHC properties at P42. Triple labeling for the adult IHC marker Slc7a14, tdTomato, and Ctbp2 showed that, unlike the OHCs in control mice (Fig. 4*A–A‴*), in Slc26a5-Tbx2 mice, Slc7a14 was expressed in the tdTomato+ cIHCs (#2, Fig. 4*B–B‴* orange arrows), albeit at a markedly lower level relative to the IHCs (#1, Fig. 4*B–B‴*, blue arrowheads). Notably, endogenous OHCs not expressing tdTomato did not express Slc7a14 (#3, Fig. 4*B–B‴*, blue arrows) and also did not express Ctbp2 in their nuclei, whereas nuclear Ctbp2 expression in cIHCs (#2) was as high as that in endogenous IHCs (#1).

We measured the nuclear diameter and quantified the Ctbp2+ puncta in IHCs (#1, 314 cells), cIHCs (#2, 296 cells), and endogenous OHCs (#3, 385 cells) in the same region in Slc26a5-Tbx2 mice at P42 ($n = 3$): Nuclei in cIHCs reached the size of nuclei in IHCs and were significantly (***$p < 0.001$) larger than OHC nuclei (Fig. 4*C*); conversely, Ctbp2+ puncta (2.54 ± 0.34) in cIHCs were significantly (****$p < 0.0001$) fewer than in IHCs (16.24 ± 0.12; Fig. 4*D*). We also examined the expression pattern of Otoferlin, another IHC marker that was only expressed in IHCs in control mice at P42 (Fig. 4*E–E″*). As expected, Otoferlin was expressed in tdTomato+ cIHCs (Fig. 4*F–F″*, orange arrows) but absent in endogenous OHCs not expressing tdTomato (Fig. 4*F–F″*, blue arrows).

To test whether Ikzf2, a key TF for stabilizing the OHC fate (Chessum et al., 2018), was repressed in cIHCs, we exploited the *Ikzf2*$^{V5/+}$ model, in which three V5 tags are fused at the Ikzf2 C-terminus (Bi et al., 2022; S. Li et al., 2023). V5 (Ikzf2) was expressed in all OHCs but not IHCs in control *Ikzf2*$^{V5/+}$ mice (Fig. 4*G–G″*), and V5 (Ikzf2) expression was also not detected in vGlut3+ cIHCs in *Slc26a5*$^{CreER/+}$; *Rosa26*$^{Tbx2/+}$; *Ikzf2*$^{V5/+}$ (Slc26a5-Tbx2-*Ikzf2*$^{V5/+}$ in brief) mice (Fig. 4*H–H″*, orange arrows); in contrast, endogenous OHCs not expressing vGlut3 maintained V5 (Ikzf2) expression (Fig. 4*H–H″*, blue arrows). Moreover, we also noticed that V5 (Ikzf2) was not expressed in cochlear SCs at P5 (Fig. 4*I–I‴*) but became detectable in SCs at P30 (Fig. 4*J–J‴*). Notably, the expression level

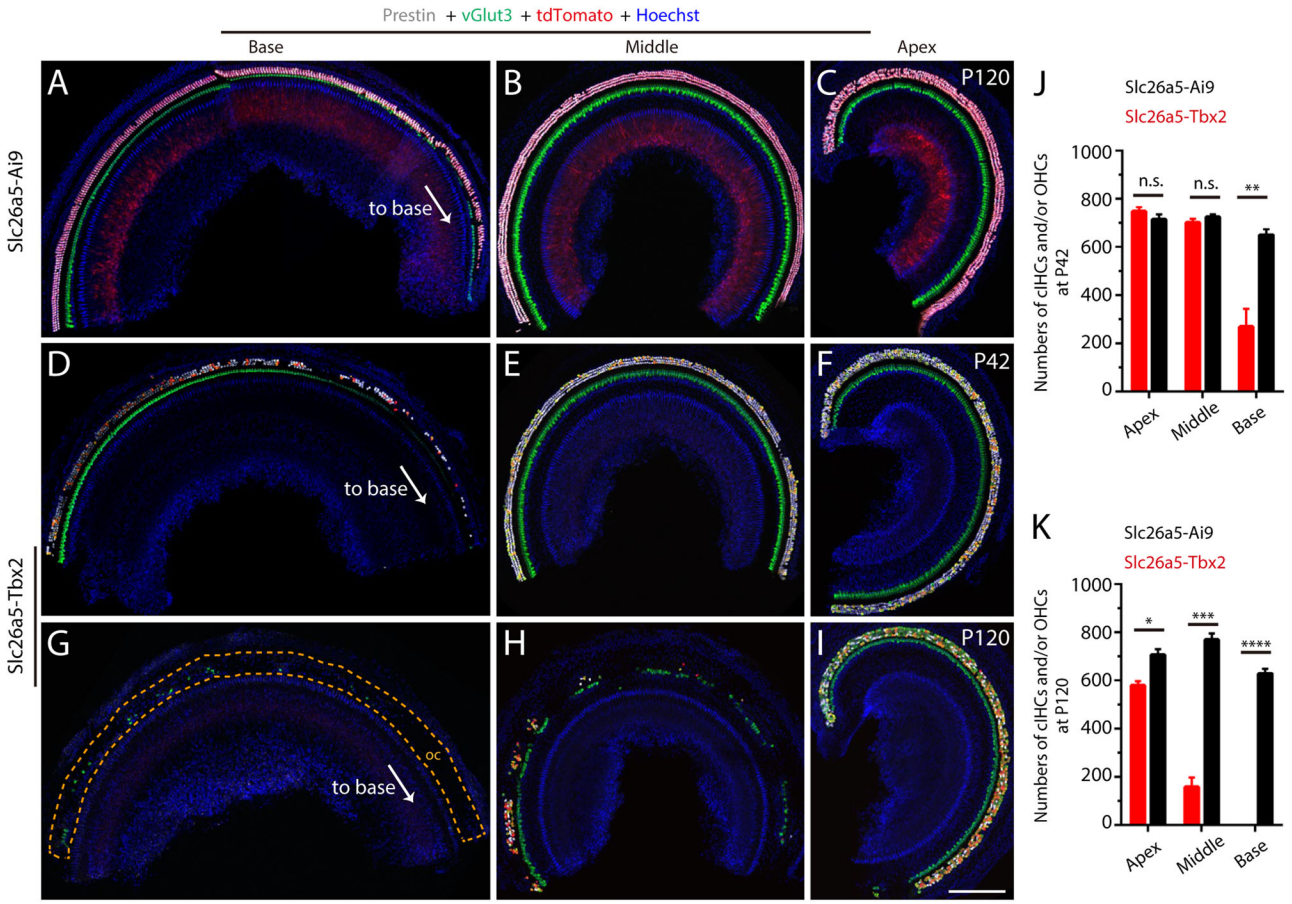

Figure 3. HCs are degenerated in Slc26a5-Tbx2 mice. ***A–I***, Triple labeling for Prestin, vGlut3, and tdTomato in control Slc26a5-Ai9 mice ($n = 3$) at P120 (***A–C***) and Slc26a5-Tbx2 mice at P42 (***D–F***, $n = 3$) and P120 (***G–I***, $n = 3$). In control mice, HC degeneration is mild and only in the most basal portion (***A***), whereas in Slc26a5-Tbx2 mice, the cIHCs or OHCs start degenerating in a basal-to-apical gradient: The degeneration primarily occurs in the basal turn (***D***) at P42 and then extends to the middle turn (***H***) at P120, with the HC degeneration in the apical turn remaining mild at P120 (***I***). IHCs are normal at P42 (***D–F***), but severe IHC loss is detected in basal (***G***) and middle (***H***) turns but not the apical turn (***I***) at P120. The tdTomato signal medial to IHCs in control mice (***A–C***) is the background signal, which is manifest in mice over 2 months old and also present in Ai9/+ mice at P120. ***J***, ***K***, Quantification of the remaining cIHCs and/or OHCs in apical, middle, and basal turns separately in control (black) and Slc26a5-Tbx2 (red) mice at P42 (***J***) and P120 (***K***). Data are presented as means ± SEM. Student's *t* test was used for statistical analysis. $*p < 0.05$; $**p < 0.01$; $***p < 0.001$; $****p < 0.0001$; ns, not significant. Scale bar: 200 µm (***I***).

of Ikzf2 in SCs appeared weaker than that in OHCs at P30. Thus, Ikzf2 protein expression was not exclusive to OHCs. Because Ikzf2 was never detected in IHCs, it was more of a non-IHC marker. Collectively, these data further supported the notion that cIHCs gained, albeit not completely, IHC features and lost OHC characteristics, particularly Ikzf2 expression.

The cIHCs lose electromotility, and hearing capacity is severely impaired in Slc26a5-Tbx2 mice at P42

We performed patch-clamp recording on four cell types at P42: (1) WT_OHCs (#1, $n = 6$ cells) and (2) WT_IHCs (#2, $n = 5$) from WT mice and (3) endogenous OHCs (#3, $n = 11$) not expressing tdTomato and (4) tdTomato+ cIHCs (#4, $n = 9$) from the same Slc26a5-Tbx2 mice (Fig. 5*A*). Unlike in the two types of OHCs (#1 green and #3 blue), nonlinear capacitance (NLC) was not detected in WT_IHCs (#2, black) and cIHCs (#4, Fig. 5*A*, red). Total Prestin was calculated by Qmax, the maximum charge transfer that is closely associated with Prestin population within the membrane (Fig. 5*A*, the area below green and blue NLC curves). The calculated total Prestin amount in cIHCs was also significantly ($****p < 0.0001$) lower than that in WT_OHCs (Fig. 5*B*), which agreed with the immunostaining results showing that Prestin expression was markedly decreased or completely lost in the cIHCs (Fig. 2). We also found that the NLC or Prestin level in OHCs (#3, blue) was slightly ($*p < 0.05$) lower than that in WT_OHCs (#1, green); this might be due to the endogenous OHCs (#3) being affected, to certain extent, by the nearby cIHCs (#4), although these OHCs maintained their OHC fate and high Prestin expression (Fig. 2). Moreover, by measuring the linear capacitance, we calculated the total cell surface area of the four cell types (Fig. 5*C*). Cell surface area was not significantly different between WT_OHCs (#1) and OHCs (#3; Fig. 5*C*). Because IHCs are known to be larger and feature a greater cell surface area than OHCs (Romand et al., 2000), we predicted that the cell surface of cIHCs would be larger than that of OHCs. Unexpectedly, the total cell surface area of cIHCs (#4) was comparable to that of OHCs (#3; Fig. 5*C*), although the nuclei of the cIHCs were larger than those of OHCs (Fig. 4*C*). We speculated that the length or height of the cIHCs might be decreased, relative to OHCs. Such speculation was supported by the overall 3D morphologies of the cIHCs visualized by the IMRIS software (Movie 1).

Consistently, auditory brainstem response (ABR) measurement revealed that, at P42, the hearing thresholds at all tested frequencies in Slc26a5-Tbx2 mice ($n = 7$) were significantly ($****p < 0.0001$ or $**p < 0.01$) increased relative to those in

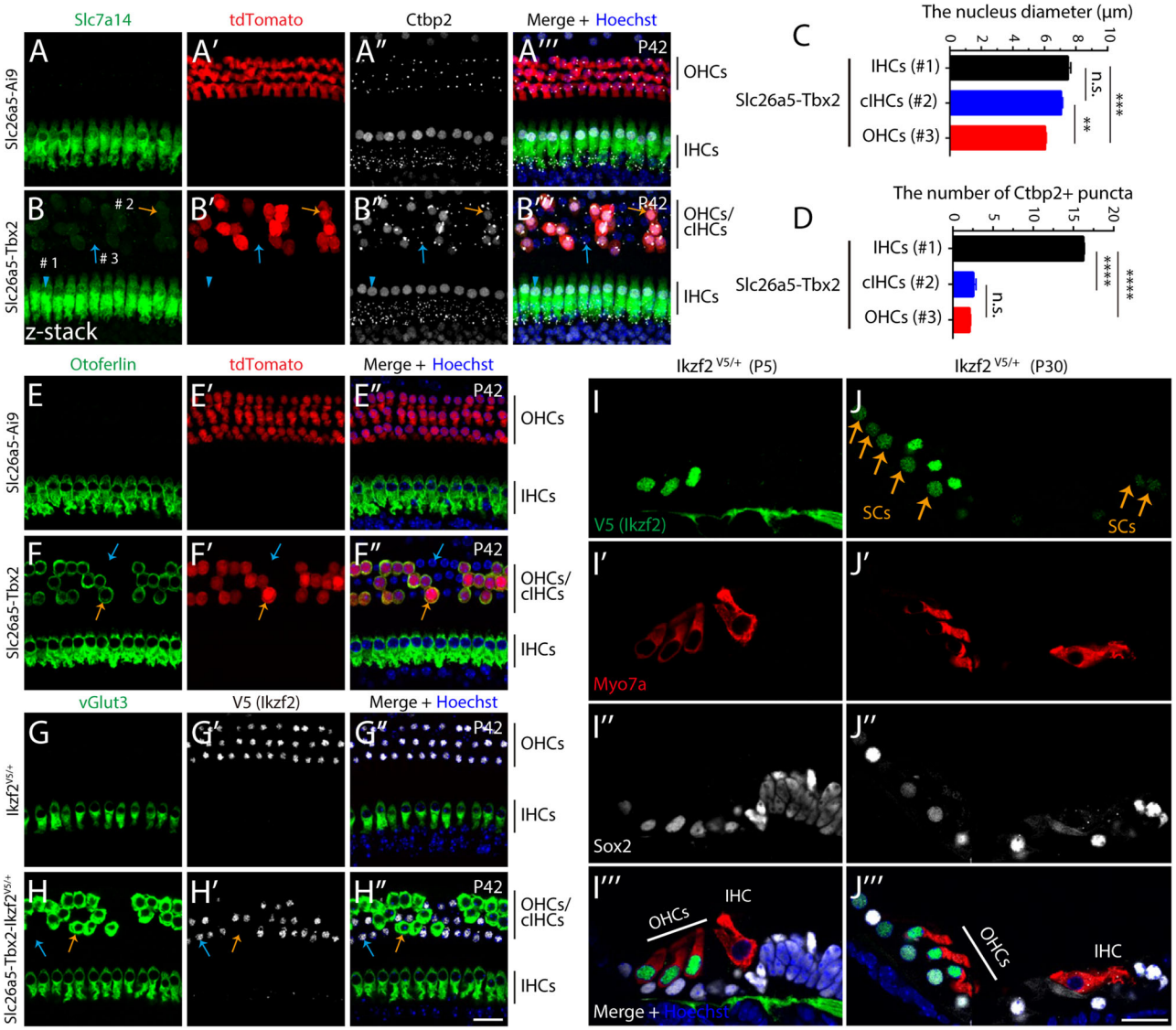

Figure 4. cIHCs gain other IHC features and lose Ikzf2 protein expression. ***A***, ***B‴***, Triple labeling for Slc7a14, tdTomato, and Ctbp2 in control Slc26a5-Ai9 mice (***A–A‴***, $n = 3$) and Slc26a5-Tbx2 mice (***B–B‴***, $n = 3$) at P42. Blue arrowheads (#1, ***B–B‴***): one IHC. Orange arrows (#2, ***B–B‴***): one tdTomato+/Slc7a14+ cIHC expressing Ctbp2 in the nucleus. Blue arrows (#3, ***B–B‴***): one endogenous OHC not expressing tdTomato (Tbx2), Slc7a14, and Ctbp2 in the nucleus. ***C***, ***D***, Comparison of cell types #1, #2, and #3 in (***B–B‴***) for nuclear diameter (***C***) and number of Ctbp2+ puncta (***D***). Data are presented as means ± SEM. One-way ANOVA is used for statistical analysis. $^{**}p < 0.01$; $^{***}p < 0.001$; $^{****}p < 0.0001$; n.s., not significant. ***E***, ***F′***, Colabeling of Otoferlin and tdTomato in Slc26a5-Ai9 mice (***E–E″***, $n = 3$) and Slc26a5-Tbx2 mice (***F–F′***, $n = 3$) at P42. Orange arrows (***F–F′***): one tdTomato+/Otoferlin+ cIHC. Blue arrows (***F–F′***): one endogenous OHC expressing neither tdTomato nor Otoferlin. ***G***, ***H″***, Colabeling of vGlut3 and V5 (Ikzf2) in control *Ikzf2*$^{V5/+}$ mice (***G–G″***, $n = 3$) and Slc26a5-Tbx2-Ikzf2$^{V5/+}$ mice (***H–H′***, $n = 3$) at P42. Orange arrows (***H–H″***): one cIHC expressing vGlut3 but lacking V5 (Ikzf2) expression. Blue arrows (***H–H″***): one endogenous OHC maintaining Ikzf2 expression and not expressing vGlut3. ***I***, ***J‴***, Triple staining of V5 (Ikzf2), Myo7a and Sox2 in cryosection cochlear tissues of *Ikzf2*$^{V5/+}$ mice at P5 (***I–I‴***) and P30 (***J–J‴***). Ikzf2 is expressed in OHCs at P5, but not in IHCs and SCs. In contrast, besides OHCs, Ikzf2 is also detected in SCs (arrows in ***J–J‴***), albeit at a lower level compared with OHCs. Scale bar: 20 μm (***H″***, ***J‴***).

WT mice ($n = 5$; Fig. 5*D*), implying severe impairment of hearing capacity. Finally, a scanning electron microscope (SEM) assay showed that hair bundles of cIHCs became disorganized or fused in Slc26a5-Tbx2 mice, compared with OHCs in the WT control mice at P42 (Fig. 5*E,F*). The degeneration of hair bundles became more severe at P120 (Fig. 5*G,H*). The hair bundles of cIHCs were degenerated (Fig. 5*H*, green color) or completely lost (Fig. 5*H*, white dotted circle) in Slc26a5-Tbx2 mice at P120; in contrast, the hair bundles of OHCs in Slc26a5-Tbx2 mice (Fig. 5*H*, pink color) appeared largely normal. Collectively, these results suggest that Tbx2 misexpression converted neonatal OHCs into cIHCs that lost Prestin-mediated electromotility, displayed degenerated hair bundles, or underwent cell death, leading to severe hearing impairment.

Gene expression profile differs significantly between WT OHCs and IHCs at adult ages

Our analysis above suggested that cIHCs were not equivalent to IHCs. To further bolster this notion, we performed single-cell transcriptomic profiling to determine the degree of cell fate conversion in cIHCs. We have previously reported the single-cell RNA-seq profile of 17 WT OHCs at P30 (P30_WT OHCs old; S. Sun et al., 2021) and 50 WT IHCs at P30 (P30_WT IHCs; Bi et al., 2022). To balance the numbers of IHCs and OHCs, we additionally picked 32 WT OHCs at P30 (P30_WT OHCs new) from Slc26a5-Ai9 mice. Upon mixing all IHCs and OHCs, we found, as expected, that the new and old P30_WT OHCs overlapped in clustering analysis (Fig. 6*A*); thus, the new and old P30_WT OHCs were grouped together as

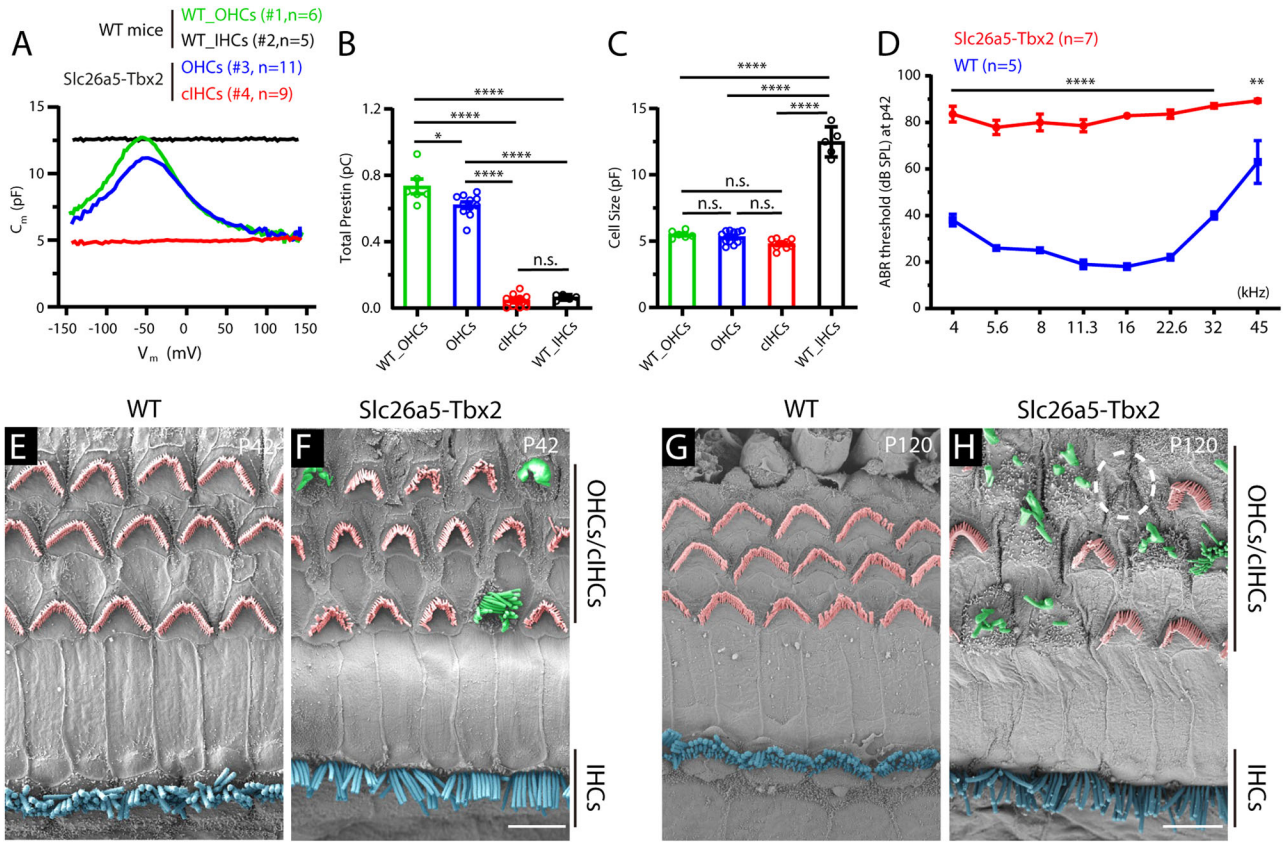

Figure 5. cIHCs lose electromotility and their hair bundles are degenerated. ***A***, Nonlinear capacitance (NLC) measurement of OHCs (#1, green, $n = 6$, cell number) and IHCs (#2, black, $n = 5$) in wild-type (WT) mice at P42, as well as of endogenous OHCs not expressing tdTomato/Tbx2 (#3, blue, $n = 11$) and cIHCs expressing tdTomato/Tbx2 (#4, red, $n = 9$). Notably, #3 and #4 are from the same Slc26a5-Tbx2 mice at P42, which could be distinguished by the presence or absence of tdTomato. ***B***, ***C***, Comparing total Prestin amount (***B***) and cell size (***C***) among the four cell types in (***A***). Data are presented as means ± SEM. See Movie 1 for more details. Statistical analysis was performed using one-way ANOVA. *$p < 0.05$, ****$p < 0.0001$; n.s., not significant. ***D***, ABR measurement of WT ($n = 5$) and Slc26a5-Tbx2 ($n = 7$) mice at P42. Hearing is significantly impaired in Slc26a5-Tbx2 mice at all tested frequencies. Data are presented as means ± SEM. Student's *t* test was used for statistical analysis. **$p < 0.01$; ****$p < 0.0001$. ***E***, ***H***, SEM analysis of WT ($n = 3$, ***E***, ***G***) and Slc26a5-Tbx2 ($n = 3$, ***F***, ***H***) mice at P42 (***E***, ***F***) and P120 (***G***, ***H***). Degenerated hair bundles of cIHCs are shown in green; white dotted circle: one cIHC that has either died or lost its hair bundles. Scale bar: 5 µm (***F***, ***H***).

P30_WT OHCs. Importantly, we performed the gene expression profiling of all cells by using smart-seq, which can yield high gene coverage because it represents full-length RNA-seq (Ramskold et al., 2012).

Both P30_WT OHCs and P30_WT IHCs shared the pan-HC markers *Pou4f3* and *Myo7a* (Fig. 6*B*,*C*). Moreover, the IHC markers *Slc17a8*, *Slc7a14*, and *Tbx2* were enriched in P30_WT IHCs (Fig. 6*D*–*F*; Ruel et al., 2008; Seal et al., 2008; Bi et al., 2022; Giffen et al., 2022), whereas the OHC markers *Slc26a5*, *Ikzf2*, and *Lbh* were enriched in P30_WT OHCs (Fig. 6*G*–*I*; Zheng et al., 2000; Liberman et al., 2002; Chessum et al., 2018; H. Liu et al., 2021). Comprehensive comparison of the transcriptomic profiles between P30_WT OHCs and P30_WT IHCs revealed that 2,010 genes were expressed at significantly different levels [absolute value of fold-change (FC) > 4, $p < 0.05$], with 1,482 genes enriched in P30_WT IHCs and 528 genes enriched in P30_WT OHCs (Extended Data Fig. 6-1), which were defined as IHC and OHC genes, respectively. The top differentially expressed genes were presented in the heatmap in Figure 6*J*.

Cell fate conversion in cIHCs is largely incomplete

We next used the same smart-seq approach and examined 67 tdTomato+ cIHCs manually picked from Slc26a5-Tbx2 mice at P42, which we defined as P42_cIHCs. We picked the cells at P42, instead of at P30, to provide the cells a longer duration to transform; this was because these cells were derived from endogenous OHCs at P2/P3 rather than from control OHCs that start differentiation from embryonic ages. The P42_cIHCs were mixed with P30_WT IHCs and P30_WT OHCs, and then clustering analysis was performed. Although the P42_cIHCs were closer to P30_WT IHCs than to P30_WT OHCs, three distinct cell clusters were formed (Fig. 7*A*,*B*). Nevertheless, the P42_cIHCs expressed pan-HC markers (*Myo7a*, *Pou4f3*, and *Tmc1*) and IHC markers (*Slc17a8*, *Slc7a14*, and *Tbx2*), but did not express or minimally expressed OHC markers (*Slc26a5*, *Ikzf2*, and *Lbh*; Fig. 7*C*–*E*). Notably, *Tbx2* levels appeared higher in P42_cIHCs than in P30_WT IHCs (Fig. 7*E*), which might be due to both ectopic (from *Rosa26* locus) and endogenous *Tbx2* being transcribed in P42_cIHCs. Moreover, global gene expression correlation coefficient analysis revealed that P42_cIHCs resembled P30_WT IHCs >P30_WT OHCs, although a manifest difference existed between P42_cIHCs and P30_WT IHCs (Fig. 7*F*).

To estimate the extent of divergence of the cIHCs from OHCs, we compared the global gene expression profiles between P42_cIHCs and P30_WT OHCs. Compared to the P30_WT OHCs, the expression levels of 2,061 genes were dramatically (FC > 4, and $p < 0.05$) upregulated (Fig. 8*A*, right side), whereas 459 genes were downregulated in P42_cIHCs (Fig. 8*A*, left side). We found that 1,268 genes overlapped between the 2,061 upregulated genes and the 1,482 IHC-specific genes (Extended

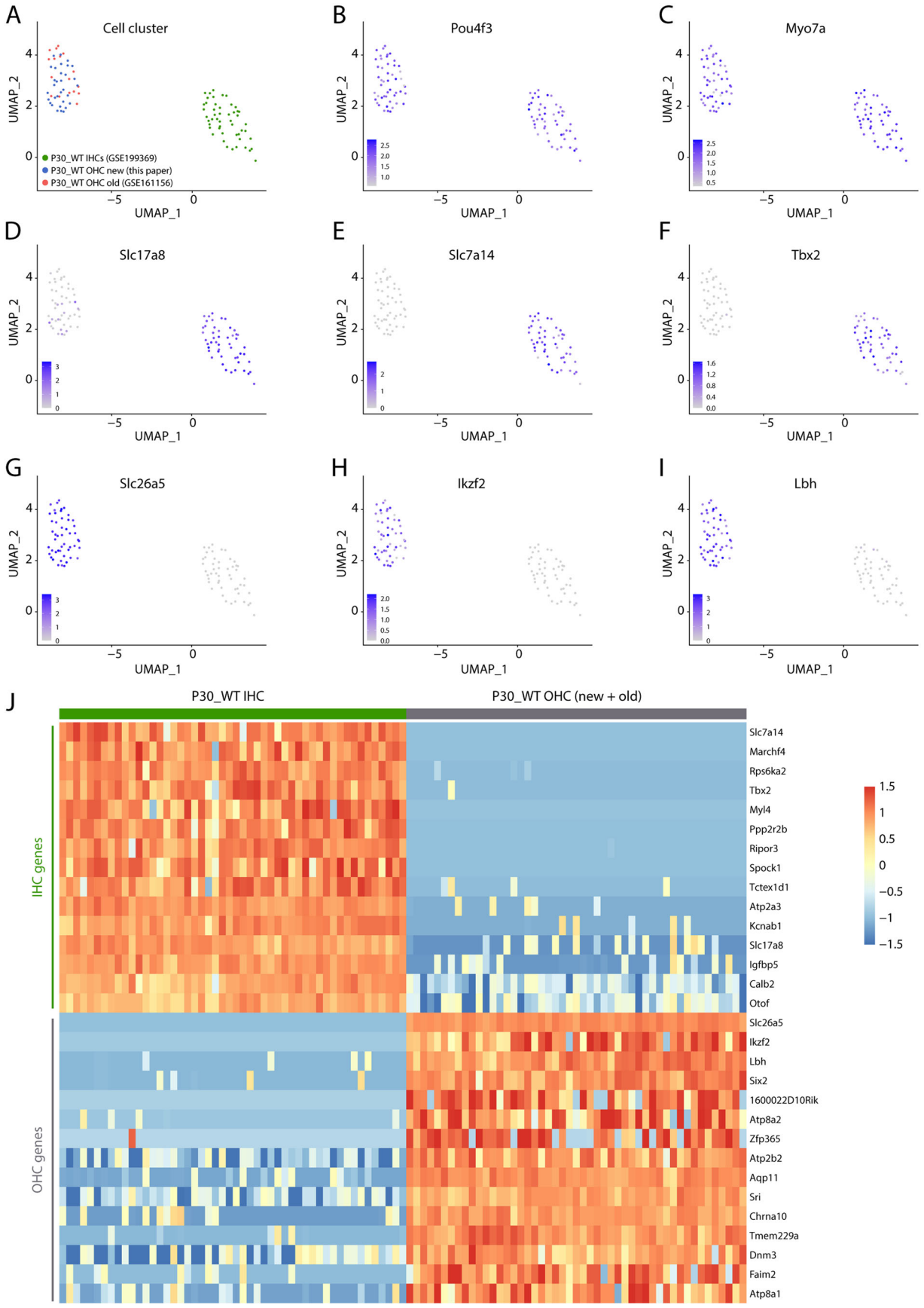

Figure 6. Transcriptomic difference between wild-type (WT) OHCs and IHCs at P30. ***A***, Clustering of mixed cell population comprising our newly picked P30_WT OHCs new (blue, 32 cells) and previously reported P30_WT OHCs old (red, 17 cells) and P30_WT IHCs (green, 50 cells). P30_WT OHCs new and P30_WT OHCs old are clustered together and divergent from P30_WT IHCs. ***B–I***, In addition to pan-HC markers *Pou4f3* (***B***) and *Myo7a* (***C***), IHC markers *Slc17a8* (***D***), *Slc7a14* (***E***), and *Tbx2* (***F***), as well as OHC markers *Slc26a5* (***G***), *Ikzf2* (***H***), and *Lbh* (***I***), are shown in cells presented in (***A***). ***J***, Heatmap of top genes showing significantly differential levels between P30_WT IHCs and P30_WT OHCs. See Extended Data Figure 6-1 for more details.

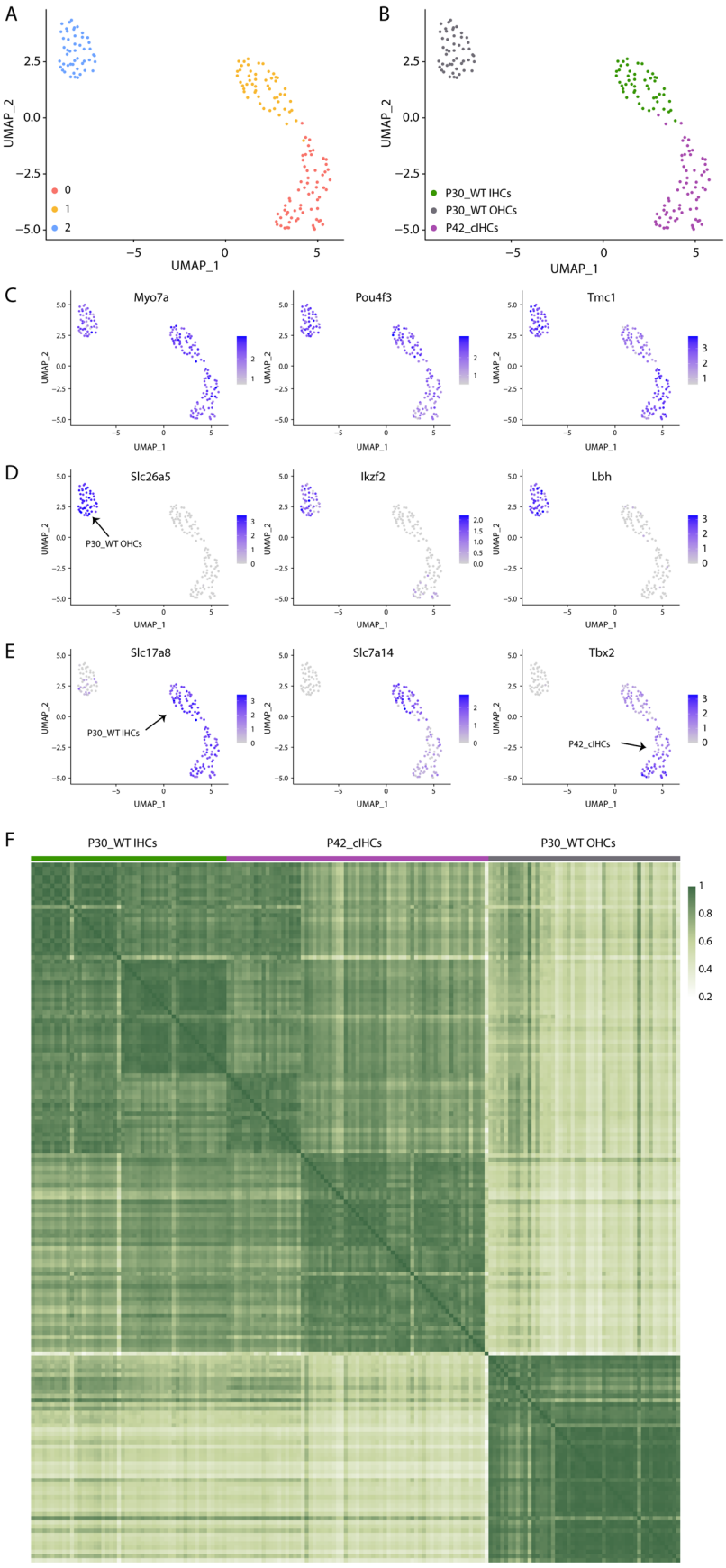

Figure 7. The cIHCs minimally overlap with the WT IHCs. ***A***, ***B***, The cell population, a mixture of P30_WT IHCs, P30_WT OHCs, and P42_cIHCs, subject to unsupervised clustering (***A***) or marked by cell identity (***B***). ***C–E***, Clustering of cell population including P30_WT OHCs, P30_WT IHCs, and P42_cIHCs, plotted with pan-HC marker genes *Myo7a*, *Pou4f3*; and *Tmc1* (***C***), OHC-specific genes *Slc26a5*, *Ikzf2*, and *Lbh* (***D***); and IHC-specific genes *Slc17a8*, *Slc7a14*, and *Tbx2* (***E***). Arrow in ***D***: P30_WT OHCs. Arrow in ***E***, left: P30_WT IHCs. Arrow in ***E***, right: P42_cIHCs. ***F***, Correlation coefficient analysis of P30_WT OHCs, P30_WT IHCs, and P42_cIHCs. Global gene expression profiles of P42_cIHCs diverge from those of P30_WT OHCs and instead become similar—but remain far from fully equivalent—to those of P30_WT IHCs.

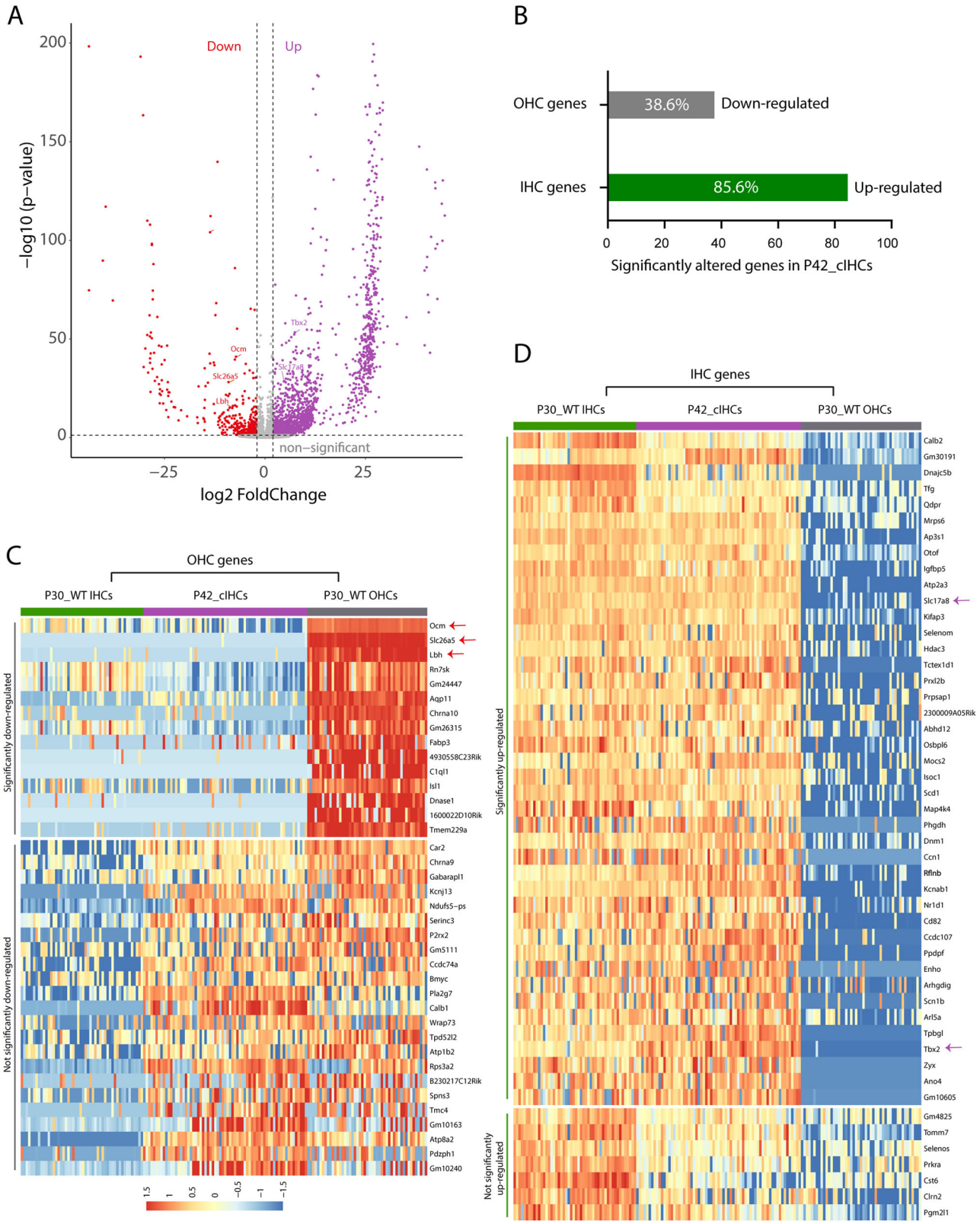

Figure 8. Full-length single-cell transcriptomic analysis of wild-type (WT) IHCs, OHCs, and cIHCs at adult ages. ***A***, ***B***, Transcriptomic comparison reveals that 459 genes are significantly downregulated and 2,061 genes are upregulated in the P42_cIHCs, compared with the P30_WT OHCs (***A***). Among the 459 downregulated genes, 204 are OHC-specific genes, occupying 38.6% of the total OHC genes (***B***). Likewise, among the 2,061 upregulated genes, 1,268 are IHC unique genes, representing 85.6% of the IHC unique genes. ***C***, Heatmap of significantly (top part) and not significantly (bottom part) downregulated OHC genes. ***D***, Heatmap of top significantly (top part) and not significantly (bottom part) upregulated IHC genes. See Extended Data Figures 8-1 and 8-2 for more details.

Data Fig. 6-1) and that, similarly, among the 459 downregulated genes, 204 overlapped with the 528 OHC-specific genes (Extended Data Fig. 6-1). Thus, 85.6% (1,268/1,482) of IHC genes were markedly increased, and 38.6% (204/528) of OHC genes were significantly decreased in P42_cIHCs (Fig. 8*B*). The top significantly or not significantly altered OHC and IHC genes were presented in heatmaps in Figure 8, *C* and *D*, and the entire gene list was included in Extended Data Figure 8-1. These results suggested that IHC genes were more readily (or more efficiently) upregulated than OHC genes are downregulated. Gene ontology (GO) analysis showed that genes involved in cell adhesion, intracellular signaling transduction, protein localization to the plasma membrane, cell migration, and phosphorylation were enriched in the 1,268 IHC genes upregulated in the P42_cIHCs. Among the IHC genes not significantly increased in the P42_cIHCs, genes involved in response to xenobiotic stimulus were overrepresented. Likewise, angiogenesis-related genes were enriched in the OHC genes that were not significantly downregulated in the P42_cIHCs. In contrast, no gene category was overrepresented in the OHC genes that were significantly downregulated in the P42_cIHCs. The full gene names of the above GO terms were listed in Extended Data Figure 8-2.

Collectively, our data support the conclusion that Tbx2 alone cannot completely overwrite the OHC transcriptional program and convert OHCs into bona fide "IHCs"; instead, the cIHCs likely exist, more or less, in a hybrid state coexpressing several genes that are otherwise expressed in a mutually exclusive manner in IHCs or OHCs in WT mice.

Embryonic HC progenitors overexpressing Tbx2 develop into IHC-like cells with abnormal hair bundles

We now sought to ascertain whether Tbx2 misexpression at embryonic ages would completely transform the HC progenitors, particularly those that would normally adopt the OHC fate, into IHCs; thus, we analyzed the strain $Atoh1^{Cre/+}$; $Rosa26^{Tbx2/+}$ (Atoh1-Tbx2 in brief). Almost all HCs and a small fraction of SCs are targeted in $Atoh1^{Cre/+}$ (Yang et al., 2010). We confirmed that ectopic nuclear HA (Tbx2) expression was not detected in the HCs of control $Atoh1^{Cre/+}$ mice (Fig. 9*A–A*‴) but was present in the HCs of Atoh1-Tbx2 cochleae (Fig. 9*B–B*‴, arrows). Moreover, we focused on Fgf8, a specific marker for nascent and differentiating IHCs (Jacques et al., 2007; Ratzan et al., 2020); Fgf8 expression can be faithfully represented by GFP in the KI mouse strain *Fgf8*-P2A-3 × GFP/+ ($Fgf8^{GFP/+}$ in brief; Pan et al., 2023), and we analyzed here control $Atoh1^{Cre/+}$; $Fgf8^{GFP/+}$ (Atoh1-Fgf8 in short) mice and experimental $Atoh1^{Cre/+}$; $Rosa26^{Tbx2/+}$; $Fgf8^{GFP/+}$ (Atoh1-Tbx2-Fgf8 in short) mice at P2. Bcl11b is a specific marker for nascent and differentiating OHCs (Wiwatpanit et al., 2018; Luo et al., 2022). Triple labeling for GFP, tdTomato, and the early OHC-marker Bcl11b revealed that GFP (Fgf8) and Bcl11b were exclusively expressed in IHCs and OHCs, respectively (Fig. 9*C–C*‴). In contrast, all tdTomato+ cells in the OHC region had lost Bcl11b expression and started to express GFP (Fgf8) in Atoh1-Tbx2-Fgf8 mice (Fig. 9*D–D*‴, arrows). These GFP+/tdTomato+/Bcl11b− cells in the OHC region were defined as cIHCs. We further analyzed $Atoh1^{Cre/+}$ and $Atoh1^{Cre/+}$; $Rosa26^{Tbx2/+}$ (Atoh1-Tbx2) mice at P7. Unlike in control $Atoh1^{Cre/+}$ mice, in which Prestin was exclusively expressed in OHCs and vGlut3 was specific to IHCs (Fig. 9*E–E*‴), in Atoh1-Tbx2 mice, Prestin expression was completely absent in the tdTomato+ cIHCs, which instead expressed vGlut3 (Fig. 9*F–F*‴, arrows). The tdTomato+ IHCs here appeared normal (Fig. 9*D–D*‴,*F–F*‴, arrowheads), supporting that additional Tbx2 expression in IHCs did not significantly affect their differentiation.

Intriguingly, we observed that the alignment of cIHCs was not as regular as that of OHCs in control mice, particularly at P7 (Fig. 9*F–F*‴). Accordingly, SEM analysis revealed that, relative to OHC hair bundles (Fig. 9*G*, pink color) in control $Atoh1^{Cre/+}$ mice at P7, the overall planar cell polarity (PCP) of hair bundles among the cIHCs was defective (Fig. 9*H*, green color). Nonetheless, each cIHC lost the V- or W-shaped hair bundle and gained the bird wing-shaped hair bundle (Bi et al., 2022; X. Li et al., 2023), similar to the endogenous IHCs (Fig. 9*H*, blue color). Because $Atoh1^{Cre/+}$ also targets a fraction of pillar cells (PCs) and Deiters' cells (DCs; Yang et al., 2010), we also determined the effect of ectopic Tbx2 on the lateral two SC subtypes, pillar cells (PCs) and Deiters' cells (DCs), that normally do not express Tbx2 (Bi et al., 2022). Consistent with previous reports (Bermingham-McDonogh et al., 2006; Fritzsch et al., 2010; Nishimura et al., 2017; Luo et al., 2021), Prox1 was specifically expressed in PCs and DCs at P2 (Fig. 10*A–A*‴). However, among the 209 tdTomato+ PCs and DCs from Atoh1-Tbx2 mice ($n = 4$), all of them lost Prox1 expression but maintained expression of pan-SC marker Sox2 (Fig. 10*B–B*‴,*C*, arrows). It suggests that gene expression patterns of PCs and DCs were altered by Tbx2, agreeing with the previous report that Tbx2 overexpression converts the lateral SCs to medial SCs (Kaiser et al., 2022). Collectively, our results showed that in the presence of ectopic Tbx2 starting at embryonic ages, cochlear development in the lateral portion was grossly defective, and we did not observe four rows of bona fide "IHCs."

Tbx2 misexpression in adult OHCs can repress Prestin and derepress vGlut3 expression

Whether Tbx2 misexpression can perturb gene expression in adult OHCs has remained completely unknown. Here, Slc26a5-Tbx2 mice were administered tamoxifen at P60 and P61 and then analyzed at P90 or P120 (Fig. 11*A*), in parallel with control Slc26a5-Ai9 mice. Different from the control (Fig. 11*B–B*‴), vGlut3 was induced and Prestin was repressed in the tdTomato+ cells at P90 that were also defined as cIHCs (Fig. 11*C–C*‴). Both vGlut3 and Prestin were expressed at heterogeneous levels among the tdTomato+ cIHCs. Nevertheless, there was a negative correlation between the expression levels of vGlut3 and Prestin (Fig. 11*C–C*‴, compare the orange arrow and arrowheads). This contrasting pattern between vGlut3 and Prestin expression agreed with the unsynchronized and various incomplete stages of cIHCs along the roadmap of OHC-to-IHC conversion. Notably, the heterogeneity had largely disappeared at P120 (Fig. 11*D–D*‴). All tdTomato+ cIHCs highly expressed vGlut3 but lacked or faintly expressed Prestin (Fig. 11*D–D*‴, orange arrowheads). As expected, OHCs not expressing tdTomato harbored the highest level of Prestin and did not express detectable vGlut3 at P90 and P120 (Fig. 11*C–D*‴, blue arrows).

To simplify quantification of our results, according to the confocal immunostaining signals, we roughly divided cIHCs into two categories, $vGlut3^{Low}/Prestin^{High}$ (Fig. 11*C–C*‴, orange arrows) and $vGlut3^{High}/Prestin^{Low}$ (Fig. 11*C–D*‴, orange arrowheads), with "low" including both faint and undetectable protein expression. Among all tdTomato+ cIHCs, 67.95% ± 4.87% ($n = 3$ mice) were $vGlut3^{Low}/Prestin^{High}$, and 32.77% ± 4.48% ($n = 3$) were $vGlut3^{High}/Prestin^{Low}$ at P90, whereas almost all (98.75% ± 1.25%; $n = 3$) were $vGlut3^{High}/Prestin^{Low}$ at P120 (Fig. 11*E,F*). Thus, our results supported that Tbx2 misexpression alone was

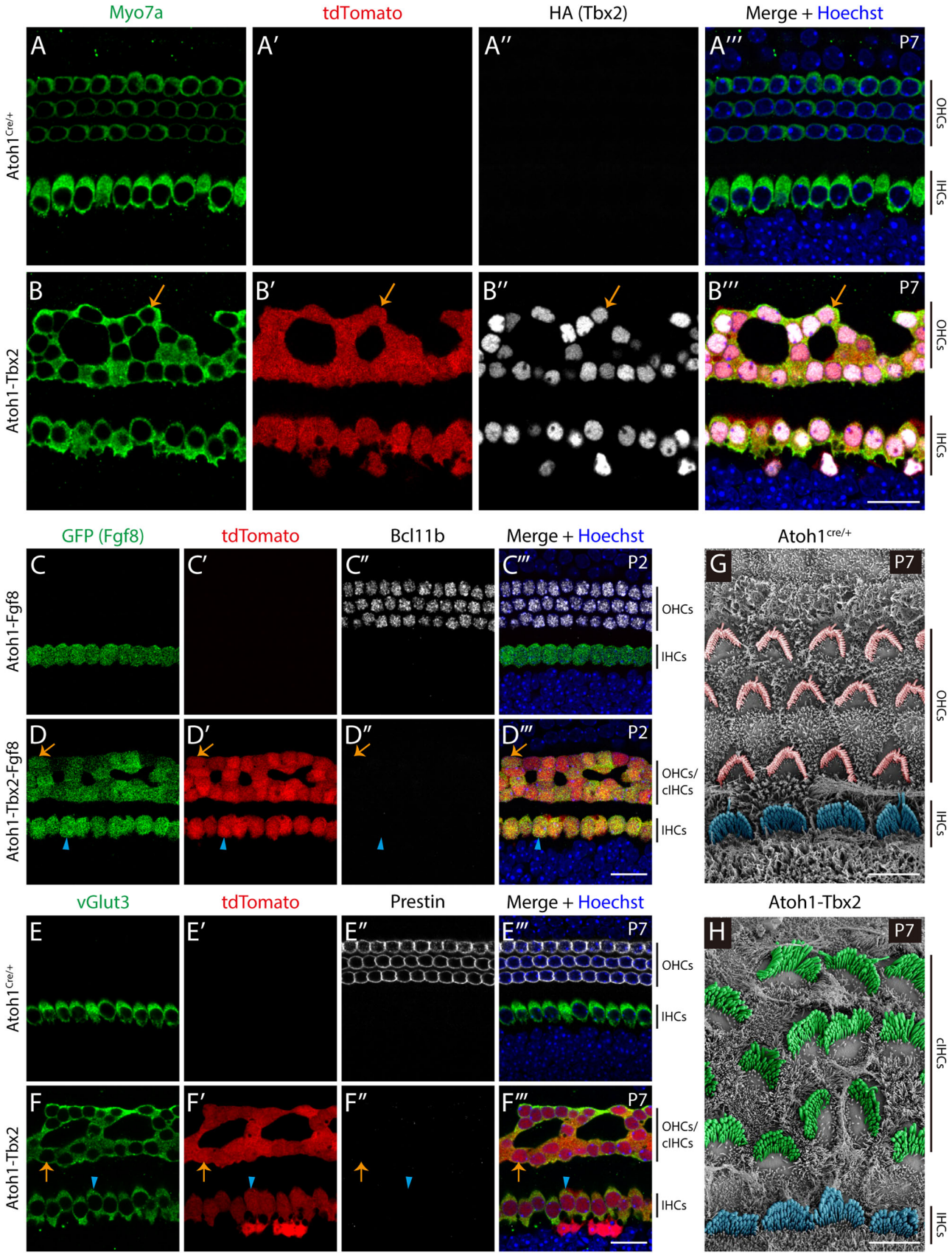

Figure 9. Tbx2 misexpression converts lateral cochlear progenitors into IHC-like cells with disorganized hair bundles. ***A–B‴***, Triple labeling for Myo7a, tdTomato, and HA (Tbx2) in control *Atoh1*$^{Cre/+}$ mice (***A–A‴***, $n = 3$) and Atoh1-Tbx2 mice (***B–B‴***, $n = 3$) at P7. Expression of tdTomato and HA (Tbx2) is tightly paired and only detected in Atoh1-Tbx2 mice (***B–B‴***). All tdTomato+ cells are HA (Tbx2)+, and vice versa. Orange arrows: one cIHC expressing Myo7a, tdTomato, and HA (Tbx2). As expected, HA (Tbx2) is distributed in HC nuclei. ***C–D‴***, Triple labeling for GFP (Fgf8), tdTomato, and OHC-marker Bcl11b in cochlear samples from control Atoh1-Fgf8 mice ($n = 3$, ***C–C‴***) and experimental Atoh1-Tbx2-Fgf8 mice ($n = 3$, ***D–D‴***) at P2. Orange arrows in (***D–D‴***): same cIHC expressing GFP (Fgf8) and tdTomato but lacking Bcl11b. Blue arrowheads: one IHC expressing GFP (Fgf8) and tdTomato but not Bcl11b. ***E–F‴***, Triple labeling for vGlut3,

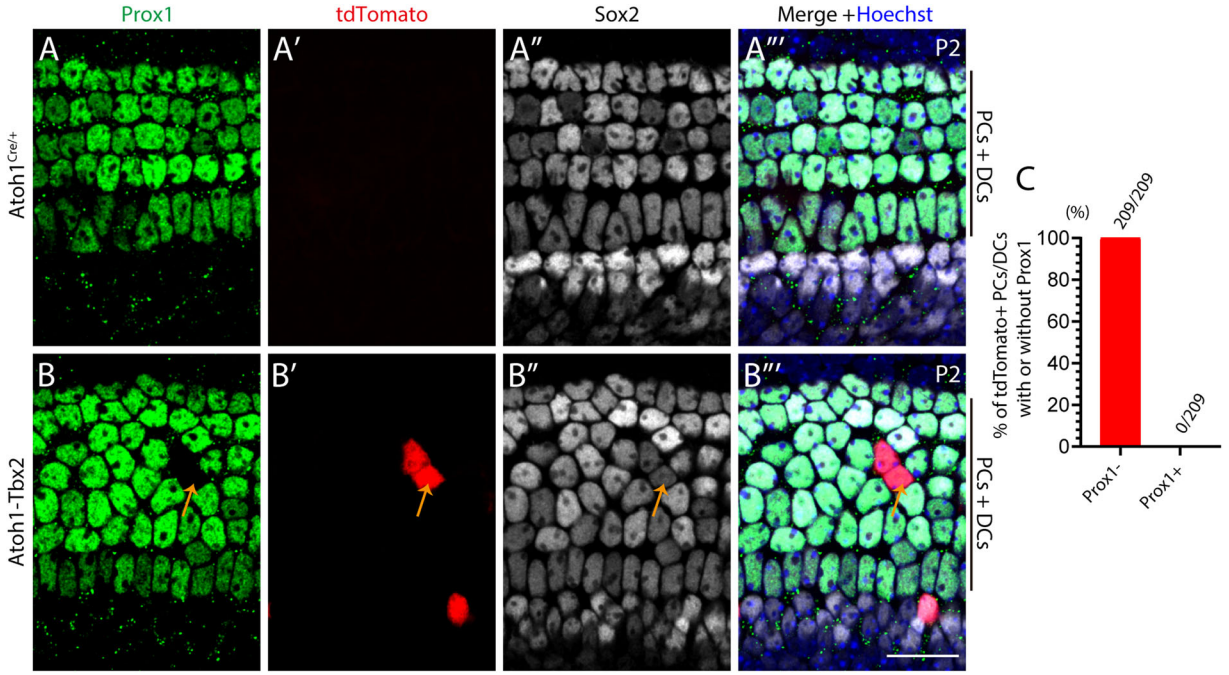

Figure 10. Ectopic Tbx2 causes defective development of cochlear SCs. ***A***, ***B***, Triple staining of Prox1, tdTomato, and Sox2 in control *Atoh1*$^{Cre/+}$ (***A–A‴***, $n = 3$) and Atoh1-Tbx2 mice (***B–B‴***, $n = 3$) at P2. The orange arrows in (***B–B‴***) mark one tdTomato+ cell (in the DC region) that loses Prox1 but maintains Sox2 expression. ***C***, Percentage of the tdTomato+ (Tbx2+) PCs and DCs that express or do not express Prox1 at P2. All of the 209 tdTomato+ PCs and DCs lose Prox1 expression. Scale bar: 20 µm (***B‴***).

sufficient to perturb, at least partly, the gene expression pattern in adult OHCs.

Construction of a new mouse strain in which Tbx2 and Ikzf2 can be overexpressed concurrently

The molecular mechanism by which Tbx2 destabilizes the OHC fate is unknown. In cIHCs, the expression of both *Ikzf2* mRNA and protein was repressed (Figs. 4*H–H*”, 7*D*). Because Ikzf2 is necessary for consolidating the OHC fate (Chessum et al., 2018; S. Li et al., 2023), we hypothesized that Ikzf2 repression by Tbx2 is one of the key contributors to cIHC production. We tested this hypothesis by determining whether Ikzf2 restoration can mitigate the effects of Tbx2 overexpression on OHCs.

To ensure that Ikzf2 expression is concurrently restored in all OHCs overexpressing Tbx2, we constructed a new mouse line, *Rosa26*-CAG-Loxp-stop-Loxp-Tbx2*3 × HA-P2A-Ikzf2*3 × V5-T2A-EGFP/+ (*Rosa26*$^{Tbx2\text{-}Ikzf2/+}$ in brief; Fig. 12*A–C*). Southern blotting revealed that no random insertion of the targeting vector occurred in the mouse genome (Fig. 12*D*), and the WT and heterozygous KI *Rosa26*$^{Tbx2\text{-}Ikzf2/+}$ mice could be readily identified using tail-DNA PCR (Fig. 12*E*). After Cre-mediated recombination, OHCs expressing Tbx2 and Ikzf2 were expected to be EGFP+, as confirmed below.

Ikzf2 restoration antagonizes the effects of Tbx2 on OHC-IHC conversion

By analyzing *Slc26a5*$^{CreER/+}$; *Rosa26*$^{Tbx2\text{-}Ikzf2/+}$ (Slc26a5-Tbx2-Ikzf2 in brief) mice at P42, we confirmed that all EGFP+ cells in the OHC region expressed nuclear HA (Tbx2) and V5 (Ikzf2; Fig. 12*F–F‴*, orange arrows); in contrast, the EGFP- OHCs did not express nuclear HA (Tbx2) or V5 (Ikzf2; Fig. 12*F–F‴*, blue arrows), with the membrane HA signal here being contributed by the HA-tagged Prestin in *Slc26a5*$^{CreER/+}$ mice (Fang et al., 2012). We continued defining these EGFP+ cells in the Slc26a5-Tbx2-Ikzf2 model as cIHCs, although these cIHCs were expected to be distinct from the cIHCs in the Slc26a5-Tbx2 model above.

Lastly, we performed triple labeling for vGlut3, tdTomato (or EGFP), and Prestin in these three models that were administered tamoxifen at P2 and P3 (Fig. 13*A*): (1) Slc26a5-Ai9 (Fig. 13*B–B‴*); (2) Slc26a5-Tbx2 (Fig. 13*C–C‴*); and (3) Slc26a5-Tbx2-Ikzf2 (Fig. 13*D–D‴*). The first two models have been described above and served here only as controls. Briefly, two lines of evidence supported our conclusion that Ikzf2 markedly, albeit not completely, antagonized the effects of Tbx2 on neonatal OHCs. First, vGlut3 expression in all EGFP+ cIHCs was drastically decreased or barely detected, and the vGlut3 channel had to be overexposed to visualize the weak vGlut3 expression in IHCs (Fig. 13*D–D‴*). Second, Prestin expression was restored in 79.01% ± 5.59% of the EGFP+ cIHCs (Fig. 13*D–D‴*, orange arrows, #1), although the expression level was considerably lower than that in nearby EGFP- endogenous OHCs (Fig. 13*D–D‴*, blue arrows); Prestin was undetectable in the remaining 20.99% of the EGFP+ cIHCs (Fig. 13*D–D‴*, orange arrows, #2). Collectively, these results suggest that relative to cIHCs mis-expressing Tbx2 alone, the cIHCs with Ikzf2 restoration showed

←

tdTomato, and Prestin in cochlear tissues of control *Atoh1*$^{Cre/+}$ mice ($n = 3$, ***E–E‴***) and Atoh1-Tbx2 mice ($n = 3$, ***F–F‴***) at P7. Orange arrows in (***F–F‴***): one vGlut3+/tdTomato+/Prestin− cIHC. Blue arrowheads: one IHC. The tdTomato+ cells medial to IHCs (***F–F‴***) are supporting cells that also can be targeted but considerably less frequently than HCs, by *Atoh1*$^{Cre/+}$. ***G***, ***H***, SEM images of hair bundles in *Atoh1*$^{Cre/+}$ mice ($n = 3$, ***G***) and Atoh1-Tbx2 mice ($n = 3$, ***H***) at P7. V- or W-shaped OHC hair bundles are shown in pink (***G***), the IHC-like hair bundles of cIHCs are shown in green (***H***), and the IHC hair bundles in both models are shown in blue. Scale bars: 20 µm (***B‴***, ***D‴***, ***F‴***), 5 µm (***G***, ***H***).

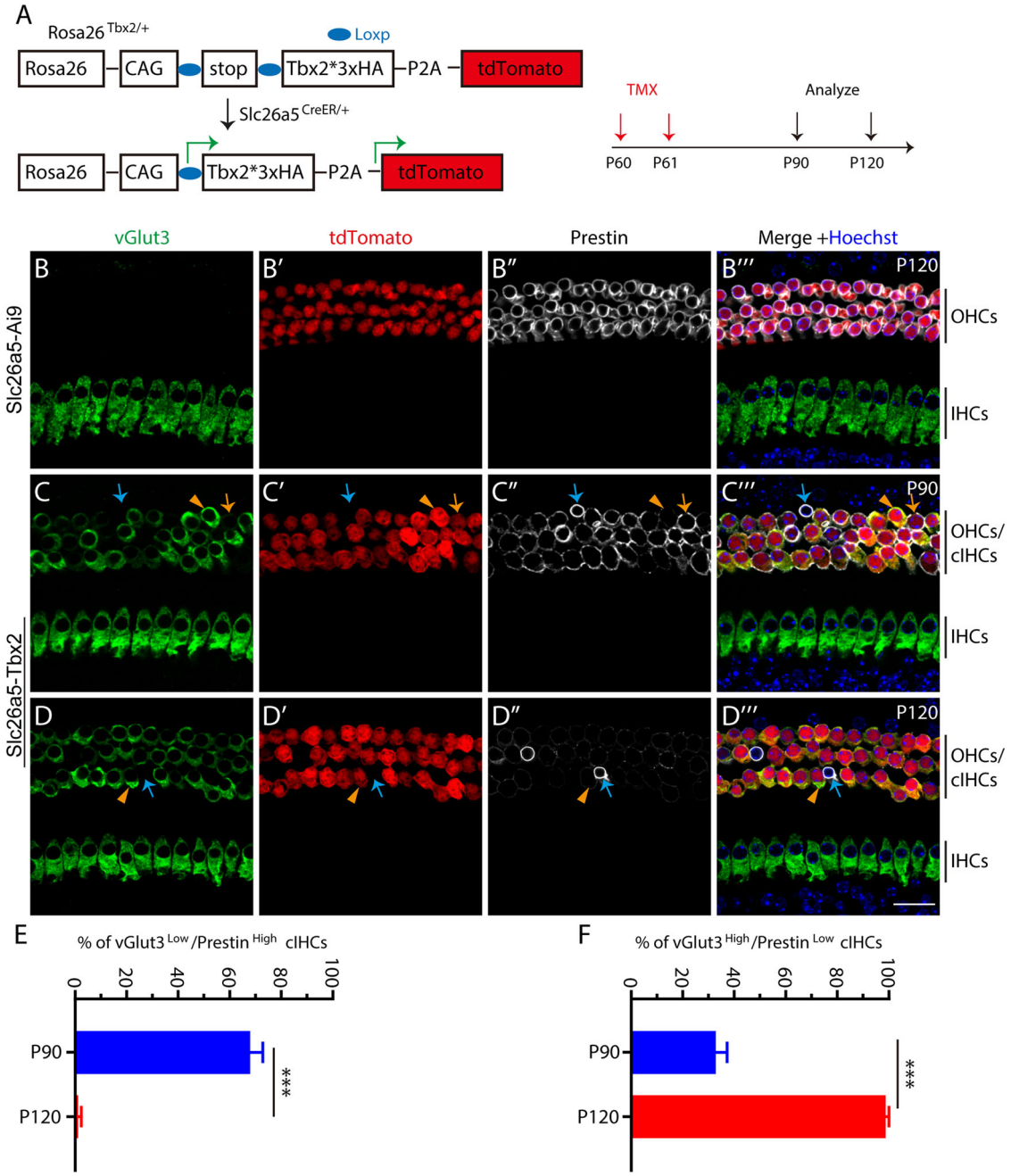

Figure 11. Tbx2 misexpression decreases Prestin expression and derepresses vGlut3 expression in adult OHCs. ***A***, A simple illustration depicting how we specifically initiate induction of Tbx2 expression in adult OHCs. ***B–D‴***, Triple labeling for vGlut3, tdTomato, and Prestin in wholemount cochlear tissues of control Slc26a5-Ai9 mice at P120 ($n = 3$, ***B–B‴***) and Slc26a5-Tbx2 mice at P90 ($n = 3$, ***C–C‴***) or P120 ($n = 3$, ***D–D‴***). All mice are administered tamoxifen at P60 and P61. Orange arrows (***C–C‴***): one tdTomato+ cIHC expressing low levels of vGlut3 but high levels of Prestin. Orange arrowheads (***C–C‴***, ***D–D‴***): tdTomato+ cIHCs expressing high levels of vGlut3 but low levels of Prestin. Blue arrows (***C–C‴***, ***D–D‴***): the endogenous OHCs that do not express tdTomato (Tbx2) and vGlut3 but maintain Prestin expression at a level as high as in endogenous OHCs in control mice (***B‴***). ***E***, ***F***, Percentages of vGlut3^{Low}/Prestin^{High} cIHCs (***E***) and vGlut3^{High}/Prestin^{Low} cIHCs (***F***). Data are presented as means ± SEM. Student's *t* test is used for statistical analysis. ***$p < 0.001$. Scale bar: 20 µm (***D‴***).

partial phenotypic reversal to a status closer to that of control OHCs, with vGlut3 expression being repressed and Prestin expression being increased (Fig. 13*E*). Thus, repression of Ikzf2 by Tbx2 misexpression is one of the key transcriptional cascades involved in destabilizing the OHC fate.

Discussion

Specification of cochlear progenitors into IHCs or OHCs

Deciphering the molecular mechanisms by which cochlear progenitors develop into IHCs or OHCs is a key prerequisite for establishing an efficient in vivo approach to regenerating HCs after trauma. The existence of pan-HC progenitors from which IHCs and OHCs are born has long been accepted (Matei et al., 2005; Driver et al., 2013), and these pan-HC progenitors are considered to generally express higher levels of Atoh1 than the progenitors that otherwise would become SCs (S. Li et al., 2022). However, recent transcriptomic and genetic evidence has led to a second proposal, according to which IHCs share the same progenitors with SCs on the medial side, whereas OHCs and lateral SCs are derived from the same progenitors (Basch et al., 2016; Kolla et al., 2020). The second proposal is further supported by

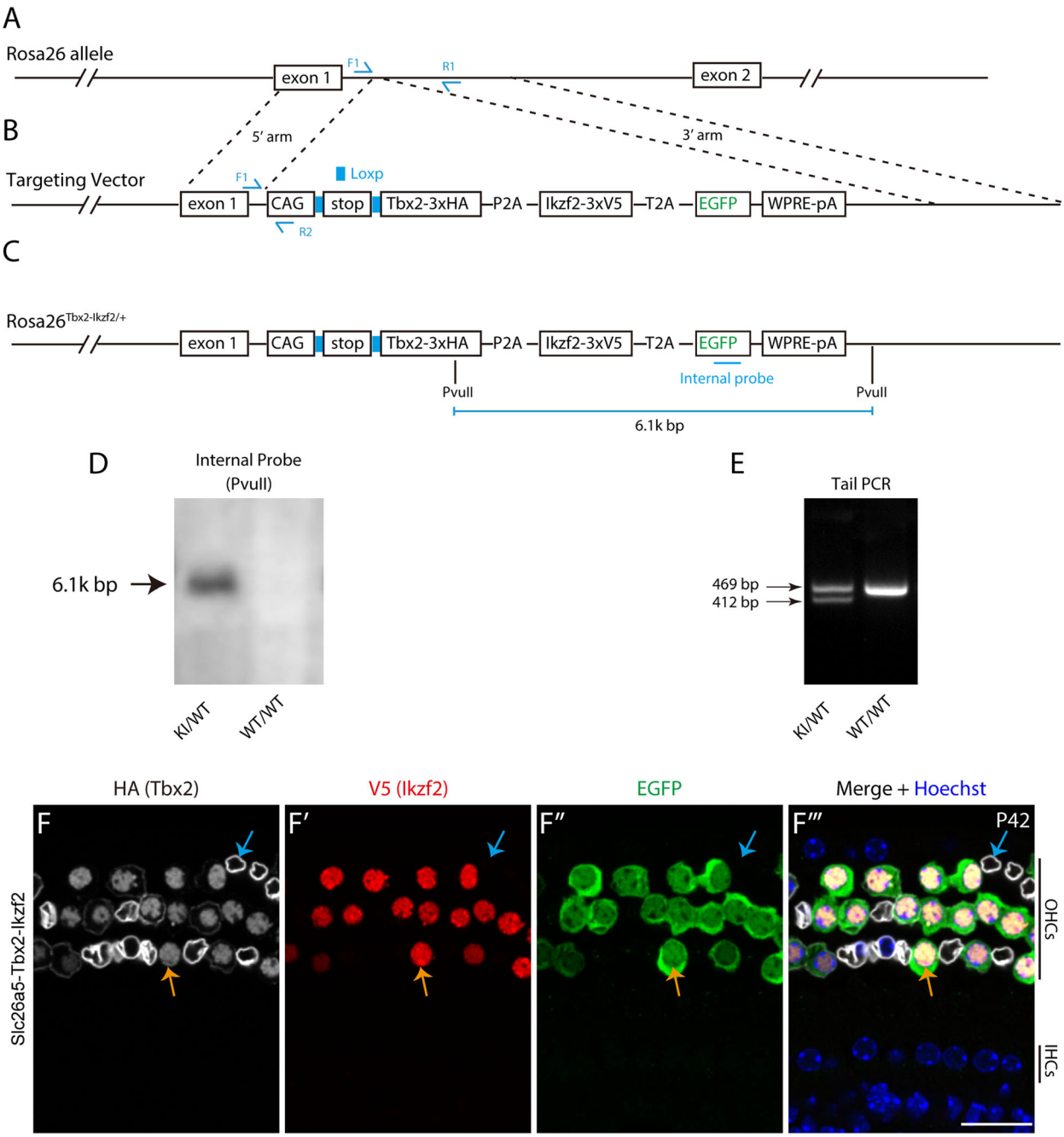

Figure 12. Construction of *Rosa26*-CAG-Loxp-stop-Loxp-Tbx2*3 × HA-P2A-Ikzf2*3 × V5-T2A-EGFP/+ (*Rosa26*$^{Tbx2\text{-}Ikzf2/+}$) strain. ***A–C***, In the wild-type *Rosa26* locus (***A***), a DNA fragment is inserted between the 5′ and 3′ arms in the targeting vector (***B***) to generate the final *Rosa26*$^{Tbx2\text{-}Ikzf2/+}$ allele (***C***). ***D***, Southern blotting with an internal probe. A 6.1k bp band is detected in heterozygous (KI/WT) but not in wild-type (WT/WT) mice. ***E***, One example gel image from tail-DNA PCR of heterozygous and wild-type mice. ***F–F‴***, Triple labeling for HA (Tbx2) and/or HA (Prestin), V5 (Ikzf2), and EGFP in Slc26a5-Tbx2-Ikzf2 mice at P42. Prestin is also tagged with HA (membrane) in *Slc26a5*$^{CreER/+}$ mice. Tbx2, Ikzf2, and EGFP show tightly paired expression. All EGFP+ cells express nuclear HA (Tbx2) and V5 (Ikzf2), and vice versa. Orange arrows: one EGFP+ cell (or cIHC) expressing V5 (Ikzf2) and nuclear HA (Tbx2). Blue arrows: one endogenous OHC expressing membrane HA-tagged Prestin but not V5 (Ikzf2) or nuclear HA-tagged Tbx2. Scale bar: 20 µm (***F‴***).

the Tbx2 expression pattern: Tbx2 is broadly expressed in cochlear cells before E13.5 but gradually downregulated, in a basal-to-apical gradient, in the lateral cochlear progenitor cells (Bi et al., 2022; Garcia-Anoveros et al., 2022; Kaiser et al., 2022); in contrast, Tbx2 is persistently expressed in medial progenitors that eventually differentiate into IHCs or SCs, including inner border cells (IBCs) and inner phalangeal cells (IPhs; Bi et al., 2022; Kaiser et al., 2022). Our current findings, together with those of previous studies (Bi et al., 2022; Garcia-Anoveros et al., 2022; Kaiser et al., 2022), support the conclusion that Tbx2 blocks the cell fates in the lateral auditory epithelium, including that of OHCs and the two nearby SC subtypes, PCs and DCs.

How does Tbx2 promote the differentiation of medial progenitors into IHCs? We propose that Tbx2+ progenitors expressing high levels of Atoh1 protein differentiate into IHCs. This is further supported by the report that Tbx2 and Atoh1 together successfully reprogram IBCs and IPhs into vGlut3+ IHCs (Bi et al.,

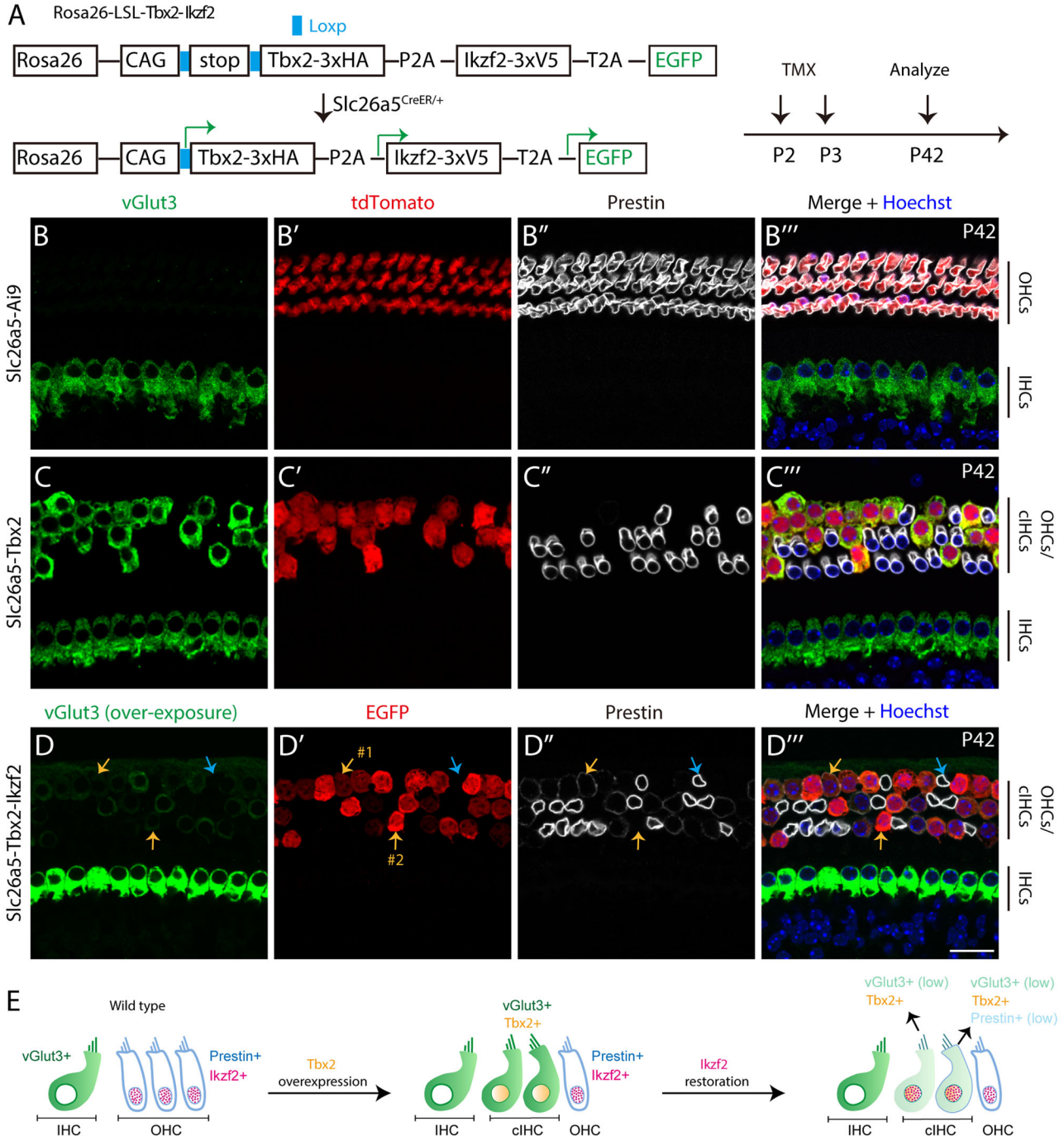

Figure 13. Ikzf2 antagonizes the effects of Tbx2 on reprogramming OHCs into cIHCs. ***A***, A simple diagram of how we concurrently induce Tbx2, Ikzf2, and EGFP expression in OHCs at P2 and P3. ***B–D‴***, Triple labeling for vGlut3, tdTomato (or EGFP), and Prestin in control Slc26a5-Ai9 (***B–B‴***, $n = 3$), Slc26a5-Tbx2 (***C–C‴***, $n = 3$), and Slc26a5-Tbx2-Ikzf2 (***D–D‴***, $n = 3$) mice at P42. vGlut3 is weakly expressed or undetectable in cIHCs in Slc26a5-Tbx2-Ikzf2 mice, and thus the vGlut3 channel has to be overexposed in IHCs in order to visualize vGlut3 in cIHCs. Orange arrows #1 (***D–D‴***): one EGFP+ cIHC with low Prestin expression. Orange arrows #2 (***D–D‴***): one EGFP+ cIHC without detectable Prestin expression. Blue arrows (***D–D‴***): one endogenous OHC not expressing EGFP (Ikzf2 and Tbx2) and maintaining Prestin expression as high as in OHCs in control mice (***B–B‴***). ***E***, The summary model highlighting that forced Ikzf2 expression in cIHCs mitigates the abnormal vGlut3 expression as well as partially restores Prestin expression in cIHCs. Scale bar: 20 µm (***D‴***).

2022). Conversely, how do Tbx2- lateral progenitors become OHCs? Because Tbx2 is downregulated before the onset of Insm1 expression in nascent OHCs (Bi et al., 2022; S. Li et al., 2023), we suspect that the absence of Tbx2 in lateral progenitors creates a permissive environment for Insm1 expression. Insm1 primarily acts as a transcriptional repressor and blocks IHC gene expression in nascent OHCs (Wiwatpanit et al., 2018). This proposal is further supported by the finding that Insm1 is derepressed in *Tbx2*$^{-/-}$ IHCs (Garcia-Anoveros et al., 2022). Thus, cochlear progenitors that express both Insm1 and high levels of Atoh1 protein become OHCs.

Molecular mechanism underlying OHC differentiation and fate maintenance at adult ages

Insm1 is expected to be only involved in the early stage of OHC development, because Insm1 is transiently expressed in nascent

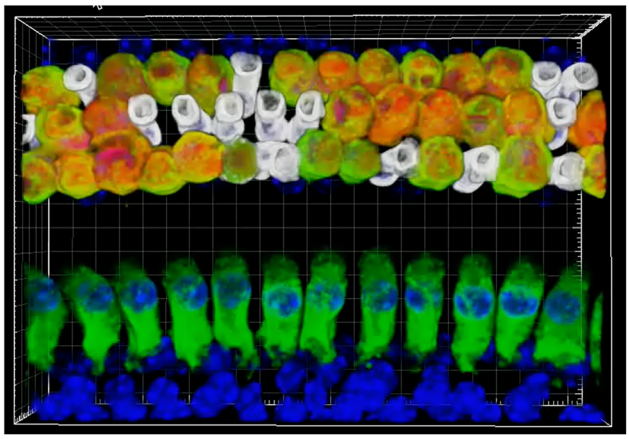

Movie 1. 3D visualization of the global morphology of the cIHCs. The raw file of confocal data is loaded into IMRIS software to readily visualize cIHCs by using orthogonal projections of the data. Red, green, and white: tdTomato, vGlut3, and Prestin signals, respectively. cIHCs express tdTomato and vGlut3, but not Prestin. Compared to OHCs, the cIHCs appear bigger but shorter. [View online]

OHCs in a basal-to-apical gradient and becomes undetectable by P2 (Lorenzen et al., 2015; S. Li et al., 2023). This raises the question of how OHC differentiation might be regulated after P2. Although this question remains largely unanswered, Ikzf2 clearly appears to play a critical role in the process: Ikzf2 expression is turned on in OHCs at ~P4 and maintained thereafter (Chessum et al., 2018; Bi et al., 2022), and the defective *Ikzf2*$^{cello/cello}$ OHCs are dysfunctional and degenerate, leading to early-onset sensorineural hearing loss (Chessum et al., 2018). Notably, we recently reported that Ikzf2 is positively but indirectly regulated by Insm1 and Ikzf2 restoration partly alleviates the abnormalities of *Insm1*$^{-/-}$ OHCs (S. Li et al., 2023). Thus, the existence of a transcriptional signaling cascade from Tbx2 to Insm1 and then from Insm1 to Ikzf2 might explain why Ikzf2 restoration can partially mitigate the effects of Tbx2 misexpression on OHCs, as revealed by our analyses (Fig. 13). However, whether Insm1 restoration also antagonizes Tbx2 misexpression in OHCs remains unknown. Another intriguing question is whether dual restoration of Insm1 and Ikzf2 might block the effects of Tbx2 overexpression on OHCs more effectively than Insm1 or Ikzf2 alone. It is also worthy of highlighting that Tbx2 expression is not IHC specific and Ikzf2 expression is not OHC specific, either, because both of them are expressed in cochlear SCs. Thus, Tbx2 is more of a non-OHC gene, and Ikzf2 is more of a non-IHC gene.

Neonatal OHCs are known to transdifferentiate into IHC-like cells upon forced Tbx2 expression (Garcia-Anoveros et al., 2022; Kaiser et al., 2022). Our study extends this finding to show that Tbx2 can destabilize the adult OHC fate, with vGlut3 upregulation and Prestin downregulation serving as readouts. Given that reprogramming fully differentiated adult cells is considerably more challenging than reprogramming their young and immature counterparts, Tbx2 can be regarded as a powerful reprogramming factor. Because *Ikzf2* conditional loss-of-function studies are lacking, the precise roles of Ikzf2 in adult OHCs remain to be determined. Ikzf2 could continue maintaining the OHC fate at adult ages, and Ikzf2 repression by Tbx2 in adult OHCs should then contribute to their perturbed gene expression.

HC degeneration in the presence of ectopic Tbx2 expression

Previous *Tbx2* gain-of-function studies have focused on whether Tbx2 can reprogram neonatal OHCs into IHCs or IHC-like cells (Garcia-Anoveros et al., 2022; Kaiser et al., 2022). The long-term effect of Tbx2 on OHCs has not been addressed. Our results here showed that cIHCs started to degenerate after P14 in a basal-to-apical gradient (Fig. 3). Why do the cIHCs undergo cell death? We suggest two possibilities: (1) The degeneration is caused by Prestin repression in the cIHCs; *Prestin*$^{-/-}$ OHCs are recognized to show normal development at early ages but then gradually degenerate at adult ages (Liberman et al., 2002). (2) Loss of Ikzf2 function leads to OHC degeneration in *Ikzf2*$^{cello/cello}$ mice (Chessum et al., 2018); thus, Ikzf2 repression could directly contribute to cIHC degeneration here. However, the precise mechanisms underlying the degeneration of both *Prestin*$^{-/-}$ and *Ikzf2*$^{cello/cello}$ OHCs remain poorly understood. Moreover, the IHCs and OHCs not overexpressing Tbx2 are also degenerated after P42, which could represent another secondary effect produced by the cell death of the cIHCs.

Tbx2 is a powerful TF but cannot fully reprogram cochlear progenitors or OHCs into IHCs

Three lines of evidence suggest that Tbx2 is a more upstream and powerful TF than Insm1 and Ikzf2 during HC development. First, whereas only ~50% of *Insm1*$^{-/-}$ OHCs become IHC-like cells (Wiwatpanit et al., 2018; S. Li et al., 2023), almost all *Tbx2*$^{-/-}$ IHCs become OHC-like cells (Bi et al., 2022). Second, *Tbx2* is epistatic to *Insm1*, and *Tbx2*$^{-/-}$; *Insm1*$^{-/-}$ IHCs transdifferentiate into OHC-like cells (Garcia-Anoveros et al., 2022). Third, Ikzf2 restoration cannot completely restore OHC features in Tbx2+ cIHCs (Fig. 13). Recently, the mechanism by which Tbx2 binds to specific DNA sequences and its associated cofactors have been reported in other cellular contexts (Lu et al., 2021). However, such a dataset for Tbx2 in cochlear cells is not available yet.

Five results presented herein support the conclusion that Tbx2 cannot fully reprogram other cochlear cell types into bona fide IHCs: (1) Our full-length single-cell transcriptomic analysis revealed that only 38.6% of OHC genes were significantly repressed in cIHCs (Fig. 8) and manifest global gene expression differences existed between cIHCs and IHCs (Fig. 7); (2) cIHCs harbored degenerated hair bundles or lacked hair bundles (Fig. 5); (3) overall cochlear development was disrupted when Tbx2 was overexpressed in cochlear sensory progenitors, with the cIHCs displaying disorganized hair bundles (Fig. 9); (4) considerably fewer ribbon synapses were present in cIHCs than in endogenous IHCs (Fig. 4); and (5) total cell surface area of cIHCs was comparable to that of OHCs and was dramatically smaller than that of WT IHCs (Fig. 5). Thus, we speculate that, although Tbx2 is one of the key IHC fate determinants, additional genes are necessary to fully reprogram OHCs or HC progenitors into IHCs, particularly into IHCs harboring well-organized IHC-like hair bundles.

References

Basch ML, et al. (2016) Fine-tuning of Notch signaling sets the boundary of the organ of Corti and establishes sensory cell fates. Elife 5:e19921.

Bermingham NA, Hassan BA, Price SD, Vollrath MA, Ben-Arie N, Eatock RA, Bellen HJ, Lysakowski A, Zoghbi HY (1999) Math1: an essential gene for the generation of inner ear hair cells. Science 284:1837–1841.

Bermingham-McDonogh O, Oesterle EC, Stone JS, Hume CR, Huynh HM, Hayashi T (2006) Expression of Prox1 during mouse cochlear development. J Comp Neurol 496:172–186.

Bi Z, Li X, Ren M, Gu Y, Zhu T, Li S, Wang G, Sun S, Sun Y, Liu Z (2022) Development and transdifferentiation into inner hair cells require Tbx2. Natl Sci Rev 9:nwac156.

Cai T, Jen HI, Kang H, Klisch TJ, Zoghbi HY, Groves AK (2015) Characterization of the transcriptome of nascent hair cells and

identification of direct targets of the Atoh1 transcription factor. J Neurosci 35:5870–5883.
Chessum L, et al. (2018) Helios is a key transcriptional regulator of outer hair cell maturation. Nature 563:696–700.
Driver EC, Sillers L, Coate TM, Rose MF, Kelley MW (2013) The Atoh1-lineage gives rise to hair cells and supporting cells within the mammalian cochlea. Dev Biol 376:86–98.
Fang J, Zhang WC, Yamashita T, Gao J, Zhu MS, Zuo J (2012) Outer hair cell-specific prestin-CreERT2 knockin mouse lines. Genesis 50:124–131.
Fritzsch B, Matei VA, Nichols DH, Bermingham N, Jones K, Beisel KW, Wang VY (2005) Atoh1 null mice show directed afferent fiber growth to undifferentiated ear sensory epithelia followed by incomplete fiber retention. Dev Dyn 233:570–583.
Fritzsch B, Dillard M, Lavado A, Harvey NL, Jahan I (2010) Canal cristae growth and fiber extension to the outer hair cells of the mouse ear require Prox1 activity. PLoS One 5:e9377.
Garcia-Anoveros J, Clancy JC, Foo CZ, Garcia-Gomez I, Zhou Y, Homma K, Cheatham MA, Duggan A (2022) Tbx2 is a master regulator of inner versus outer hair cell differentiation. Nature 605:298–303.
Giffen KP, et al. (2022) Mutation of SLC7A14 causes auditory neuropathy and retinitis pigmentosa mediated by lysosomal dysfunction. Sci Adv 8: eabk0942.
Gurdon JB, Javed K, Vodnala M, Garrett N (2020) Long-term association of a transcription factor with its chromatin binding site can stabilize gene expression and cell fate commitment. Proc Natl Acad Sci U S A 117: 15075–15084.
Jacques BE, Montcouquiol ME, Layman EM, Lewandoski M, Kelley MW (2007) Fgf8 induces pillar cell fate and regulates cellular patterning in the mammalian cochlea. Development 134:3021–3029.
Kaiser M, Wojahn I, Rudat C, Ludtke TH, Christoffels VM, Moon A, Kispert A, Trowe MO (2021) Regulation of otocyst patterning by Tbx2 and Tbx3 is required for inner ear morphogenesis in the mouse. Development 148: dev195651.
Kaiser M, Ludtke TH, Deuper L, Rudat C, Christoffels VM, Kispert A, Trowe MO (2022) TBX2 specifies and maintains inner hair and supporting cell fate in the organ of Corti. Nat Commun 13:7628.
Kim D, Langmead B, Salzberg SL (2015) HISAT: a fast spliced aligner with low memory requirements. Nat Methods 12:357–360.
Kolla L, et al. (2020) Characterization of the development of the mouse cochlear epithelium at the single cell level. Nat Commun 11:2389.
Li C, Shu Y, Wang G, Zhang H, Lu Y, Li X, Li G, Song L, Liu Z (2018) Characterizing a novel vGlut3-P2A-iCreER knockin mouse strain in cochlea. Hear Res 364:12–24.
Li X, et al. (2023) In situ regeneration of inner hair cells in the damaged cochlea by temporally regulated co-expression of Atoh1 and Tbx2. Development 150:dev201888.
Li S, Fan T, Li C, Wang Y, Li J, Liu Z (2022) Fate-mapping analysis of cochlear cells expressing Atoh1 mRNA via a new Atoh1(3*HA-P2A-Cre) knockin mouse strain. Dev Dyn 251:1156–1174.
Li S, He S, Lu Y, Jia S, Liu Z (2023) Epistatic genetic interactions between Insm1 and Ikzf2 during cochlear outer hair cell development. Cell Rep 42:112504.
Liao Y, Smyth GK, Shi W (2014) featureCounts: an efficient general purpose program for assigning sequence reads to genomic features. Bioinformatics 30:923–930.
Liberman MC, Gao J, He DZ, Wu X, Jia S, Zuo J (2002) Prestin is required for electromotility of the outer hair cell and for the cochlear amplifier. Nature 419:300–304.
Liu Z, Owen T, Zhang L, Zuo J (2010) Dynamic expression pattern of Sonic hedgehog in developing cochlear spiral ganglion neurons. Dev Dyn 239: 1674–1683.
Liu H, Giffen KP, Grati M, Morrill SW, Li Y, Liu X, Briegel KJ, He DZ (2021) Transcription co-factor LBH is necessary for the survival of cochlear hair cells. J Cell Sci 134:jcs254458.
Lorenzen SM, Duggan A, Osipovich AB, Magnuson MA, Garcia-Anoveros J (2015) Insm1 promotes neurogenic proliferation in delaminated otic progenitors. Mech Dev 138:233–245.
Love MI, Huber W, Anders S (2014) Moderated estimation of fold change and dispersion for RNA-seq data with DESeq2. Genome Biol 15:550.
Lu S, Louphrasitthiphol P, Goradia N, Lambert JP, Schmidt J, Chauhan J, Rughani MG, Larue L, Wilmanns M, Goding CR (2021) TBX2 controls a proproliferative gene expression program in melanoma. Genes Dev 35:1657–1677.
Luo Z, Zhang J, Qiao L, Lu F, Liu Z (2021) Mapping genome-wide binding sites of prox1 in mouse cochlea using the CUT&RUN approach. Neurosci Bull 37:1703–1707.
Luo Z, Du Y, Li S, Zhang H, Shu M, Zhang D, He S, Wang G, Lu F, Liu Z (2022) Three distinct Atoh1 enhancers cooperate for sound receptor hair cell development. Proc Natl Acad Sci U S A 119:e2119850119.
Matei V, Pauley S, Kaing S, Rowitch D, Beisel KW, Morris K, Feng F, Jones K, Lee J, Fritzsch B (2005) Smaller inner ear sensory epithelia in Neurog 1 null mice are related to earlier hair cell cycle exit. Dev Dyn 234:633–650.
Morsli H, Choo D, Ryan A, Johnson R, Wu DK (1998) Development of the mouse inner ear and origin of its sensory organs. J Neurosci 18:3327–3335.
Nishimura K, Noda T, Dabdoub A (2017) Dynamic expression of sox2, gata3, and prox1 during primary auditory neuron development in the mammalian cochlea. PLoS One 12:e0170568.
Pan Y, Li S, He S, Wang G, Li C, Liu Z, Xiang M (2023) Fgf8(P2A-3xGFP/+): a new genetic mouse model for specifically labeling and sorting cochlear inner hair cells. Neurosci Bull 39:1762–1774.
Pertea M, Pertea GM, Antonescu CM, Chang TC, Mendell JT, Salzberg SL (2015) StringTie enables improved reconstruction of a transcriptome from RNA-seq reads. Nat Biotechnol 33:290–295.
Ramskold D, et al. (2012) Full-length mRNA-Seq from single-cell levels of RNA and individual circulating tumor cells. Nat Biotechnol 30:777–782.
Ratzan EM, Moon AM, Deans MR (2020) Fgf8 genetic labeling reveals the early specification of vestibular hair cell type in mouse utricle. Development 147:dev192849.
Romand R, Sapin V, Ghyselinck NB, Avan P, Le Calvez S, Dolle P, Chambon P, Mark M (2000) Spatio-temporal distribution of cellular retinoid binding protein gene transcripts in the developing and the adult cochlea. Morphological and functional consequences in CRABP- and CRBPI-null mutant mice. Eur J Neurosci 12:2793–2804.
Ruel J, et al. (2008) Impairment of SLC17A8 encoding vesicular glutamate transporter-3, VGLUT3, underlies nonsyndromic deafness DFNA25 and inner hair cell dysfunction in null mice. Am J Hum Genet 83:278–292.
Seal RP, et al. (2008) Sensorineural deafness and seizures in mice lacking vesicular glutamate transporter 3. Neuron 57:263–275.
Song H, Morrow BE (2023) Tbx2 and Tbx3 regulate cell fate progression of the otic vesicle for inner ear development. Dev Biol 494:71–84.
Stuart T, Butler A, Hoffman P, Hafemeister C, Papalexi E, Mauck WM 3rd, Hao Y, Stoeckius M, Smibert P, Satija R (2019) Comprehensive integration of single-cell data. Cell 177:1888–1902.e21.
Sun S, Li S, Luo Z, Ren M, He S, Wang G, Liu Z (2021) Dual expression of Atoh1 and Ikzf2 promotes transformation of adult cochlear supporting cells into outer hair cells. Elife 10:e66547.
Sun Y, Liu Z (2023) Recent advances in molecular studies on cochlear development and regeneration. Curr Opin Neurobiol 81:102745.
Sun Y, Zhang Y, Zhang D, Wang G, Song L, Liu Z (2022) In vivo CRISPR-Cas9-mediated DNA chop identifies a cochlear outer hair cell-specific enhancer. FASEB J 36:e22233.
Tao L, Yu HV, Llamas J, Trecek T, Wang X, Stojanova Z, Groves AK, Segil N (2021) Enhancer decommissioning imposes an epigenetic barrier to sensory hair cell regeneration. Dev Cell 56:2471–2485.e5.
Wang G, Li C, He S, Liu Z (2021) Mosaic CRISPR-stop enables rapid phenotyping of nonsense mutations in essential genes. Development 148: dev196899.
Wiwatpanit T, et al. (2018) Trans-differentiation of outer hair cells into inner hair cells in the absence of INSM1. Nature 563:691–695.
Woods C, Montcouquiol M, Kelley MW (2004) Math1 regulates development of the sensory epithelium in the mammalian cochlea. Nat Neurosci 7: 1310–1318.
Yang H, Xie X, Deng M, Chen X, Gan L (2010) Generation and characterization of Atoh1-Cre knock-in mouse line. Genesis 48:407–413.
Zheng J, Shen W, He DZ, Long KB, Madison LD, Dallos P (2000) Prestin is the motor protein of cochlear outer hair cells. Nature 405:149–155.